AR6 WGI Report – List of corrigenda to be implemented

The corrigenda listed below will be implemented in the Supplementary Material during copy-editing.

CHAPTER 7 SUPPLEMENTARY MATERIAL

Document (Chapter, Annex, Supp. Mat…)	Section	Page :Line (based on the final pdf FGD version)	Detailed info on correction to make
7SM	7.SM.1.3.1	5:41	Replace "contrails, aviation induced cirrus aerosols," with "contrails and aviation-induced cirrus, aerosols,"
7SM	7.SM.1.3.1	6.5	Replace "ACCMIP" with "AeroCom"
7SM	7.SM.1.3.1	6.13 to 6.16	Delete the sentence "Newer CMIP6 model results were not used as fewer model results are available and the complexity of aerosol schemes and internal mixing in these models makes attribution of aerosol forcing to precursors more difficult than in CMIP5-era models. »
7SM	7.SM.1.3.1	6:13	Replace "Newer CMIP6 model results were not used as fewer model results are available and the complexity of aerosol schemes and internal mixing in these models makes attribution of aerosol forcing to precursors more difficult than in CMIP5-era models" by "Section 7.SM.1.3.2 explains the rationale for choosing these coefficients."
7SM	7.SM.1.3.2	7:53	After sentence "…to generate the time series of ERFari." insert "These forcing contributions are based on modelling results from Myhre et al. (2013a), with scalings and uncertainty ranges for each component selected such that the total ERFari assessment of –0.3 ± 0.3 W m^{-2} is preserved. These estimates of per-species ERFari are independent of the headline assessments in Chapter 6, and differ particularly for BC (Section 6.4.2) where total BC ERFari is assessed to be +0.145 W m^{-2}. The emulators in Chapter 7 are run with more positive ERF values for BC and more negative values for OC, SO_2 and NH_3 to preserve the assessed uncertainty range for total ERFari while maintaining a Gaussian uncertainty distribution for the forcing contribution from each species. As many aerosol precursors are co-emitted, the stronger best-estimate contributions per species used here offset each other and the time evolution and present-day values of total ERFari are broadly consistent between Chapter 6 and Chapter 7. It should be re-iterated here that the Chapter 7 values are not per-species assessments of ERFari and are used for the calibration and projection of climate in emulators."
7SM	7.SM.1.4	8:14	Replace "4.36" by "4.35"
7SM	7.SM.1.4	10:4	Replace "4.36" by "4.35"
7SM	7.SM.2.2	11:36	Insert "SPM Figure 4b," before "Chapter 1"
7SM	7.SM.2.4	12:53	Insert new subsection 7.SM.2.4: "7.SM.2.4 Supporting information for SPM Figure 4b A similar exercise was performed for the anthropogenic contributions to future warming shown in SPM Fig. 4b. As no natural forcing is included in this exercise, a long pre-industrial spin-up is not required and only the period 1750–2100 was run using the constrained two-layer model. As in Section 7.SM.2.3, 2,237 ensemble members are used, sampling the full assessed uncertainty ranges in effective radiative forcing and climate response. In these simulations, the baseline case is all anthropogenic forcing, with one component removed at a time and the differences in warming reported. Contributions to future warming are reported for CO_2, other non-CO_2

			greenhouse gases (including ozone and stratospheric water vapour from methane oxidation), and other anthropogenic components. The latter category includes aerosols, land-use change, contrails and light-absorbing particles on snow and ice. The analysis is performed for SSP1-1.9, SSP1-2.6, SSP2-4.5, SSP3-7.0 and SSP5-8.5. Temperature projections are reported for 2081–2100 relative to a 1850–1900 baseline."
7SM	7.SM.7	39	In Table 7.SM.14: Row 1, Column 1: "**Figure number / Table number / Chapter section (for calculations)"** replace with **"Figure number"**
7SM	7.SM.1	39	In Table 7.SM.14: Row 2, Column 7: "https://github.com/chrisroadmap/ar6" replace with "https://github.com/IPCC-WG1/Chapter-7"
7SM	7.SM.1	39	In Table 7.SM.14: Row 3, Column 7: "https://github.com/chrisroadmap/ar6" replace with "https://github.com/IPCC-WG1/Chapter-7"
7SM	7.SM.1	39	In Table 7.SM.14: Row 4, Column 7: "https://github.com/chrisroadmap/ar6" replace with "https://github.com/IPCC-WG1/Chapter-7"
7SM	7.SM.1	39	In Table 7.SM.14: Row 5, Column 7: "https://github.com/chrisroadmap/ar6" replace with "https://github.com/IPCC-WG1/Chapter-7"
7SM	7.SM.1	39	In Table 7.SM.14: Row 6, Column 7: "https://github.com/chrisroadmap/ar6" replace with "https://github.com/IPCC-WG1/Chapter-7"
7SM	7.SM.1	39	In Table 7.SM.14: Row 2, Column 6: Delete "(Smith et al., 2021)"
7SM	7.SM.1	39	In Table 7.SM.14: Row 4, Column 6: Delete "(Smith et al., 2021)"
7SM	7.SM.1	39	In Table 7.SM.14: Row 4, Column 6: Delete "(Smith et al., 2021)"
7SM	7.SM.1	40	In Table 7.SM.14: Row 1, Column 7: "https://github.com/chrisroadmap/ar6" replace with "https://github.com/IPCC-WG1/Chapter-7"
7SM	7.SM.1	40	In Table 7.SM.14: Row 2, Column 7: "https://github.com/chrisroadmap/ar6" replace with "https://github.com/IPCC-WG1/Chapter-7"
7SM	7.SM.1	40	In Table 7.SM.14: Row 3, Column 7: "https://github.com/chrisroadmap/ar6" replace with "https://github.com/IPCC-WG1/Chapter-7"
7SM	7.SM.1	40	In Table 7.SM.14: Row 4, Column 7: "https://github.com/chrisroadmap/ar6" replace with "https://github.com/IPCC-WG1/Chapter-7"
7SM	7.SM.1	40	In Table 7.SM.14: Row 5, Column 7: "https://github.com/chrisroadmap/ar6" replace with "https://github.com/IPCC-WG1/Chapter-7"
7SM	7.SM.1	40	In Table 7.SM.14: Row 6, Column 7: "https://github.com/chrisroadmap/ar6" replace with "https://github.com/IPCC-WG1/Chapter-7"
7SM	7.SM.1	40	In Table 7.SM.14: Row 2, Column 6: Delete "(Smith et al., 2021)"
7SM	7.SM.1	40	In Table 7.SM.14: Row 4, Column 6: Delete "(Smith et al., 2021)"
7SM	7.SM.1	40	In Table 7.SM.14: Row 5, Column 6: Delete "(Smith et al., 2021)"
7SM	7.SM.1	40	In Table 7.SM.14: Row 6, Column 6: Delete "(Smith et al., 2021)"
7SM	7.SM.1	46	In Table 7.SM.14: Row 2, Column 7: "https://github.com/chrisroadmap/ar6" replace with "https://github.com/IPCC-WG1/Chapter-7"
7SM	7.SM.1	46	In Table 7.SM.14: Row 3, Column 7: "https://github.com/chrisroadmap/ar6" replace with "https://github.com/IPCC-WG1/Chapter-7"
7SM	7.SM.1	46	In Table 7.SM.14: Row 5, Column 7: "https://github.com/chrisroadmap/ar6" replace with "https://github.com/IPCC-WG1/Chapter-7"
7SM	7.SM.1	46	In Table 7.SM.14: Row 2, Column 6: Delete "(Smith et al., 2021)"
7SM	7.SM.1	46	In Table 7.SM.14: Row 3, Column 6: Delete "(Smith et al., 2021)"
7SM	7.SM.1	46	In Table 7.SM.14: Row 5, Column 6: Delete "(Smith et al., 2021)"
7SM	7.SM.1	47	In Table 7.SM.14: Row 3, Column 7: "https://github.com/chrisroadmap/ar6" replace with "https://github.com/IPCC-WG1/Chapter-7"
7SM	7.SM.1	47	In Table 7.SM.14: Row 5, Column 7: "https://github.com/chrisroadmap/ar6" replace with "https://github.com/IPCC-WG1/Chapter-7"
7SM	7.SM.1	47	In Table 7.SM.14: Row 7, Column 7: "https://github.com/chrisroadmap/ar6" replace with "https://github.com/IPCC-WG1/Chapter-7"
7SM	7.SM.1	47	In Table 7.SM.14: Row 3, Column 6: Delete "(Smith et al., 2021)"
7SM	7.SM.1	47	In Table 7.SM.14: Row 5, Column 6: Delete "(Smith et al., 2021)"
7SM	7.SM.1	47	In Table 7.SM.14: Row 7, Column 6: Delete "(Smith et al., 2021)"
7SM	7.SM.1	48	In Table 7.SM.14: Row 1, Column 7: "https://github.com/chrisroadmap/ar6"

			replace with “https://github.com/IPCC-WG1/Chapter-7”
7SM	7.SM.3	Table 7.SM.4 Fourth row, fourth column (i.e ECS for upper assessed ranges)	Add “5.00”
7SM	7.SM.3	Table 7.SM.4 Fourth row, fifth column (i.e ECS for lower CICERO-SCM)	Add “2.53”
7SM			Update the Data Table with omitted data citations for climate model data.

7.SM Chapter 7: The Earth's energy budget, climate feedbacks, and climate sensitivity - Supplementary Material

Lead Authors:
Chris Smith (United Kingdom), Zebedee R. J. Nicholls (Australia), Kyle Armour (United States of America), William Collins (United Kingdom), Piers Forster (United Kingdom), Malte Meinshausen (Australia/Germany), Matthew D. Palmer (United Kingdom), Masahiro Watanabe (Japan)

Contributing Authors:
Thomas Gasser (Austria/France), Nicholas Leach (United Kingdom), Yann Quilcaille (Switzerland/France), Marit Sandstad (Norway), Mark Zelinka (United States of America)

This Supplementary Material should be cited as:
Smith, C., Z. R. J. Nicholls, K. Armour, W. Collins, P. Forster, M. Meinshausen, M. D. Palmer, M. Watanabe, 2021, The Earth's Energy Budget, Climate Feedbacks, and Climate Sensitivity Supplementary Material. In: *Climate Change 2021: The Physical Science Basis. Contribution of Working Group I to the Sixth Assessment Report of the Intergovernmental Panel on Climate Change* [Masson-Delmotte, V., P. Zhai, A. Pirani, S. L. Connors, C. Péan, S. Berger, N. Caud, Y. Chen, L. Goldfarb, M. I. Gomis, M. Huang, K. Leitzell, E. Lonnoy, J.B.R. Matthews, T. K. Maycock, T. Waterfield, O. Yelekçi, R. Yu and B. Zhou (eds.)]. Available from https://ipcc.ch/static/ar6/wg1.

Date: August 2021

Table of Contents

7.SM.1 Effective Radiative Forcing

7.SM.1.1 Simplified expressions for greenhouse gases

In Section 7.3.2 and Table 7.5, simplified expressions for the stratospheric-temperature-adjusted radiative forcing (SARF) are used to convert greenhouse gas (GHG) concentrations to radiative forcing. AR5 (Myhre et al., 2013b) used relationships first introduced in Myhre et al. (1998), providing a logarithmic dependence of carbon dioxide (CO_2) SARF on CO_2 concentrations, and square root dependencies of methane (CH_4) and nitrous dioxide (N_2O) SARF on CH_4 and N_2O concentrations. The CH_4 and N_2O relationships accounted for band overlaps between these gases. These simplified expressions for SARF were revised in Etminan et al. (2016) using updated spectroscopic data. The most notable changes were a substantial revision in the methane RF of about +25% to account for previously neglected shortwave effects (Section 7.3.2.2) and inclusion of the mutual band overlap between carbon dioxide and nitrous oxide (Section 7.3.2.1). In Etminan et al. (2016), calculations from the Oslo line-by-line (LBL) radiative transfer model were conducted for 48 cases that co-varied concentrations of carbon dioxide, methane and nitrous oxide that spanned values from 180–2000 ppm CO_2, 340–3500 ppb CH_4 and 200–525 ppb N_2O. These ranges were selected to cover the minimum observed from ice core records during the Last Glacial Maximum to the maximum projected in the RCP8.5 scenario in the future (Meinshausen et al., 2011b; Riahi et al., 2011). Simplified relationships linking concentrations of CO_2, CH_4 and N_2O to the SARF from each gas, including overlaps, were provided from these 48 different cases that fit the original line-by-line results within a few percent.

A more accurate but complex functional fit was provided in Meinshausen et al. (2020) to the 48 Oslo LBL cases in Etminan et al. (2016). Two main advantages to the Meinshausen et al. (2020) fit are (i) the reduced error in the new fits to the original Oslo LBL results (maximum 0.11% for the CO_2 cases compared to 3.6% in Etminan et al. (2016)) and (ii) the extension of the valid range of the fits to CO_2 concentrations above 2000 ppm, which occurs in SSP5-8.5 in the future (though not RCP8.5). One drawback to the Meinshausen et al. (2020) fit compared to the original Etminan et al. (2016) fit is that the former is defined with respect to 1750 greenhouse gas concentrations, and requires a re-calculation of the coefficients to use baseline concentrations that are different from this, whereas the Etminan et al. (2016) fit is valid for any baseline concentration within their stated validity range (180–2000 ppm CO_2, 340–3500 ppb CH_4, 200–525 ppb N_2O). In general, AR6 and Chapter 7 in particular reports SARF and effective radiative forcing (ERF) relative to a 1750 baseline, negating this possible drawback, and so the Meinshausen et al. (2020) relationships are used for computing SARF and ERF throughout Chapter 7 and in Annex III. The relationships converting concentrations to SARF are shown in Table 7.SM.1. For halogenated greenhouse gases with concentrations in the ppt range, SARF remains a linear function of concentrations, as in AR5.

[START TABLE 7.SM.1 HERE]

Table 7.SM.1: Simplified expressions to compute radiative forcing (RF) from concentrations of greenhouse gases (Myhre et al., 1998; Meinshausen et al., 2020). C, N and M refer to concentrations of CO_2 in ppm, N_2O in ppb and CH_4 in ppb, respectively.

Gas	Radiative forcing (SARF) simplified expression	Coefficients
CO_2	$C_{\alpha_{\max}} = C_0 - \frac{b_1}{2a_1}$ $\alpha' = \begin{cases} d_1 - \frac{b_1^2}{4a_1}, & C > C_{\alpha_{\max}} \\ d_1 + a_1(C - C_0)^2 + b_1(C - C_0), & C_0 < C < C_{\alpha_{\max}} \\ d_1, & C < C_0 \end{cases}$ $\alpha_{N_2O} = c_1\sqrt{N}$ $\mathrm{SARF}_{CO_2} = (\alpha' + \alpha_{N_2O}) \cdot \ln\left(\frac{C}{C_0}\right)$	$a_1 = -2.4785 \times 10^{-7}$ W m^{-2} ppm^{-2} $b_1 = 7.5906 \times 10^{-4}$ W m^{-2} ppm^{-1} $c_1 = -2.1492 \times 10^{-3}$ W m^{-2} ppb$^{-1/2}$ $d_1 = 5.2488$ W m^{-2} $C_0 = 277.15$ ppm
N_2O	$\mathrm{SARF}_{N_2O} = (a_2\sqrt{C} + b_2\sqrt{N} + c_2\sqrt{M} + d_2) \cdot (\sqrt{N} - \sqrt{N_0})$	$a_2 = -3.4197 \times 10^{-4}$ W m^{-2} ppm^{-1} $b_2 = 2.5455 \times 10^{-4}$ W m^{-2} ppb^{-1}

		$c_2 = -2.4357 \times 10^{-4}$ W m^{-2} ppb^{-1} $d_2 = 0.12173$ W m^{-2} ppb$^{-1/2}$ $N_0 = 273.87$ ppb
CH_4	$\mathrm{SARF}_{CH_4} = \left(a_3\sqrt{M} + b_3\sqrt{N} + d_3\right) \cdot \left(\sqrt{M} - \sqrt{M_0}\right)$	$a_3 = -8.9603 \times 10^{-5}$ W m^{-2} ppb^{-1} $b_3 = -1.2462 \times 10^{-4}$ W m^{-2} ppb^{-1} $d_3 = 0.045194$ W m^{-2} ppb$^{-1/2}$ $M_0 = 731.41$ ppb
Halogenated compounds and other minor GHGs	$\mathrm{SARF}_X = e_X(X - X_0)$	X and X_0 in ppb e_X is radiative efficiency (W m^{-2} ppb^{-1}) (Table 7.SM.7)

[END TABLE 7.SM.1 HERE]

7.SM.1.2 Effective radiative forcing from a doubling of CO_2

In Section 7.3.2.1, the ERF from a doubling of CO_2 ($\Delta F_{2\times CO2}$ = 3.93 W m^{-2}) is defined relative to 1750 CE concentrations of CO_2 assessed in Chapter 2 (C_0 = 278.3 ppm) and N_2O (N_0 = 270.1 ppb) using the Meinshausen et al. (2020) fits (Table 7.SM.1) to calculate SARF of 3.75 W m^{-2} and then adding an additional 5% for tropospheric adjustments (Section 7.3.2.1; Table 7.3). Using the Etminan et al. (2016) fits with the same baseline concentrations (C_0 = 278.3 ppm, N_0 = 270.1 ppb) results in a SARF of 3.80 W m^{-2} and an ERF of 3.99 W m^{-2} (Table 7.SM.2). The simplified expressions are used as no specific line-by-line experiment was performed for a doubling of CO_2 from about 1750 concentrations in Etminan et al. (2016).

Alongside the choice of simplified expression, the baseline CO_2 and N_2O concentrations also has an impact on the SARF and ERF from a doubling of CO_2 (Table 7.SM.2). Using 1850 CE baselines results in ERF values that are close, but not exactly the same, as using 1750 CE baselines (Table 7.SM.2). Using a present-day baseline results in estimates of SARF and ERF from a doubling of CO_2 that are about 1% greater than the 1750 or 1850 values (Table 7.SM.2). The 1850 baseline is significant as it the reference pre-industrial state for CMIP6 experiments, including the *abrupt4xCO2* and *1pctCO2* experiments used to estimate ECS and TCR from climate models. It should be noted that the *1pctCO2* experiment design relies on a logarithmic increase in CO_2 SARF with concentration to estimate TCR (Gregory et al., 2015), and both the Etminan et al. (2016) and Meinshausen et al. (2020) SARF formulas are super-logarithmic with increasing CO_2 concentrations.

[START TABLE 7.SM.2 HERE]

Table 7.SM.2: Computed values of the SARF of a doubling of CO_2 using the relationships in Etminan et al. (2016) and Meinshausen et al. (2020), and the ERF from a doubling of CO_2 (assessed to be SARF + 5% in Section 7.3.2.1), from different baseline concentrations of CO_2 and N_2O, and compared to SARF in AR5.

CO_2 concentration (ppm)	**N_2O concentration (ppb)**	**SARF 2×CO_2 AR5** (Myhre et al., 2013b)	**SARF 2×CO_2 (Etminan et al., 2016)**	**ERF 2×CO_2 (Etminan et al., 2016)**	**SARF 2×CO_2 (Meinshausen et al., 2020)**	**ERF 2×CO_2 (Meinshausen et al., 2020)**	**Baseline year for GHG concentrations**
278.3	270.1	3.71	3.802	3.992	3.747	**3.934**	1750 (Chapter 2 assessment)
277.15	273.87		3.801	3.991	3.746	3.933	1750 (Meinshausen et al., 2020)
284.32	273.02		3.804	3.994	3.749	3.937	1850 used in CMIP6 model integrations (Meinshausen

							et al., 2017)
389	323		3.837	4.029	3.790	3.980	2011 (Etminan et al., 2016)
409.85	332.09		3.844	4.036	3.798	3.988	2019 (Chapter 2 assessment)

[END TABLE 7.SM.2 HERE]

7.SM.1.3 Historical (1750-2019) effective radiative forcing time series

7.SM.1.3.1 Best estimate historical time series

The historical ERF time series describes how the best estimates of changes in climate drivers translates to ERF for 1750 to 2019. The time-evolution of ERF is reported separately for CO_2, CH_4, N_2O, other well-mixed greenhouse gases (WMGHGs), ozone, stratospheric water vapour from methane oxidation, contrails and aviation-induced cirrus, aerosol-radiation interactions, aerosol-cloud interactions, light-absorbing particles on snow and ice, land-use change, volcanic, and solar. The contributions from 49 halogenated GHGs comprising the "other well-mixed greenhouse gases" category are further reported individually. Data is published in Annex III.

For CO_2, CH_4 and N_2O, the SARFs are calculated using time-dependent best-estimate concentrations of these gases from Chapter 2 using the formulae in Table 7.SM.1 and using concentrations from Chapter 2 in 1750 CE as baselines (C_0 = 278.3 ppm, N_0 = 270.1 ppb, M_0 = 729.2 ppb). Tropospheric adjustments of +5% for CO_2, –14% for CH_4 and +7 % are then added to these SARF values to produce ERF (Section 7.3.2). For 49 halogenated greenhouse gases, concentration changes since 1750 are used combined with radiative efficiencies detailed in Table 7.SM.7 to derive SARF (Table 7.SM.1). Accounting for tropospheric adjustments adds +13% and +12% to CFC-11 and CFC-12 respectively when moving from SARF to ERF. No tropospheric adjustments are assumed for other halogenated species (Section 7.3.2.4).

For historical ozone forcing, the time series from 1750 to 2020 from Skeie et al. (2020) is adopted, using the multi-model mean ERF from six independent Earth System and chemistry-climate models (BCC-ESM1, CESM2-WACCM6, GFDL-ESM4, GISS-E2-1-H, MRI-ESM2-0 and Oslo-CTM3) that used CMIP6 precursor emissions and interactively calculated ozone burdens using full stratospheric and tropospheric chemistry schemes. From the original 12 models reporting results in Skeie et al. (2020), CNRM-CM6, CNRM-ESM2-1 and E3SM1-0 were excluded as they do not include full stratospheric and tropospheric chemistry, only the first out of the similar models CESM2-WACCM6 and CESM2-CAM6 were used, the input4MIPs forcing estimate (Checa-Garcia et al., 2018) was excluded as it did not use CMIP6 precursor emissions, and UKESM-1-0-LL was excluded for having implausible time evolutions of stratospheric ozone that resulted in negative total ozone ERF estimates for 2010 relative to 1850. The extrapolations for the 1750–1850 and 2010–2020 periods (run beyond 2014 using SSP2-4.5) came from a single model (Oslo-CTM3) and results were used up to and including 2019. Stratospheric water vapour from methane oxidation is treated a linear scaling of the methane ERF and scaled to the 1750–2019 assessment of 0.05 W m^{-2} (Section 7.3.2.6).

Several forcing categories (contrails, aviation-induced cirrus aerosols, and black carbon on snow) are derived from global annual emissions totals of short-lived climate forcers. For the best estimate of historical emissions from 1750 to 2019, the 11 September 2020 version of the Community Emissions Data System (CEDS) is used (Hoesly et al., 2018), obtained from https://doi.org/10.5281/zenodo.4025316. CEDS provides emissions of black carbon (BC), organic carbon (OC), sulphur dioxide (SO_2), ammonia (NH_3), nitrogen oxides (NOx), carbon monoxide (CO) and non-methane volatile organic compounds (NMVOC) from the fossil fuel, industrial and agricultural sectors. Biomass burning emissions are used from the BB4CMIP dataset (also used for CMIP6 model integrations, from Van Marle et al. (2017)), aggregated into global annual totals. The SSP2-4.5 scenario projection from BB4CMIP is used for 2015-2019.

ERF from contrails and aviation-induced cirrus uses global aviation NOx emissions as a predictor of aviation

activity following Smith et al. (2018a), and scaled to the 2018 ERF best estimate of 0.0574 W m^{-2} from Lee et al. (2020).

ERF from aerosol-radiation interactions (ERFari) was calculated by converting emissions of BC, OC, SO_2 (representing sulphate aerosol) and NH_3 (representing nitrate aerosol) to forcing using CMIP5-era ACCMIP multi-model mean contributions for each species from Myhre et al. (2013a) and scaled to obtain the assessment of –0.3 W m^{-2} for ERFari which is applied to the 2005–2014 decade. ERFari was calculated using a simple linear relationship to emissions of BC, OC, SO_2 and NH_3 (E_{BC}, E_{OC}, E_{SO2}, E_{NH3}):

$$\mathrm{ERFari} = \beta_{\mathrm{BC}}E_{\mathrm{BC}} + \beta_{\mathrm{OC}}E_{\mathrm{OC}} + \beta_{\mathrm{SO2}}E_{\mathrm{SO2}} + \beta_{\mathrm{NH3}}E_{\mathrm{NH3}} \qquad \textit{Equation 7.SM.1.1}$$

The β coefficients are selected to represent ERFari contributions of +0.3 W m^{-2} from black carbon, –0.4 W m^{-2} from sulphate, –0.09 W m^{-2} from organic carbon and –0.11 W m^{-2} from nitrate over the 2005–2014 decade, which translates to radiative efficiencies of β_{BC} = 50.8 mW yr m^{-2} MtC^{-1}, β_{OC} = –6.21 mW yr m^{-2} MtC^{-1}, β_{SO2} = –3.62 mW yr m^{-2} $MtSO_2^{-1}$, and β_{NH3} = –2.08 mW yr m^{-2} $MtNH_3^{-1}$. Newer CMIP6 model results were not used as fewer model results are available and the complexity of aerosol schemes and internal mixing in these models makes attribution of aerosol forcing to precursors more difficult than in CMIP5-era models.

ERF from aerosol-cloud interactions (ERFaci) is modelled as a logarithmic function of emissions of SO_2, BC and OC following Smith et al. (2018a):

$$\mathrm{ERFaci} = -\beta \ln(1 + E_{\mathrm{SO2}}/s_{\mathrm{SO2}} + (E_{\mathrm{BC+OC}}/s_{\mathrm{BC+OC}})) \qquad \textit{Equation 7.SM.1.2}$$

Eq. (7.SM.1.2) is based on the offline model of Ghan et al. (2013) using a functional form developed by Stevens (2015) with the inclusion of a carbonaceous aerosol term than can influence ERFaci. Eq. (7.SM.1.2) was tuned to 11 CMIP6 models that provided historical time-varying (1850-2014) ERFaci estimates and a parameter set of β, s_{SO2} and s_{BC} was obtained for each CMIP6 model. The parameter tunings from these 11 models were used to generate distributions using kernel density estimates from which 100,000 sample members were drawn and 100,000 candidate ERFaci time series were produced. The best estimate ERFaci time series is taken from the median of this 100,000-member ensemble, and then scaled to the assessed ERFaci of –1.0 W m^{-2} for 1750 to 2005–2014.

ERF from light-absorbing particles on snow is linear with BC emissions and scaled to the 1750-2019 ERF assessment of 0.08 W m^{-2}.

ERF from land-use change is broken down into an albedo component and an irrigation component. The albedo component follows the historical ERF time series from Ghimire et al. (2014) from 1700 to 2005, and is extended forward to 2019 using cumulative land-use related CO_2 emissions from the SSP Historical and SSP2-4.5 scenarios. This follows the treatment in Smith et al. (2018a) and assumes that land-use related CO_2 is closely related to deforestation and albedo change. The 1750-2019 assessment of –0.15 W m^{-2} is then applied to the time series. The ERF from irrigation, assessed to be –0.05 W m^{-2} for 1750–2019 (Sherwood et al., 2018), scales with the albedo component.

All anthropogenic components of the ERF described above are expressed relative to a 1750 baseline.

Natural forcings comprise solar changes and volcanic eruptions (forcing from galactic cosmic rays is assessed to be negligible, Section 7.3.4.5). Volcanic ERF is derived from stratospheric aerosol optical depth (SAOD) using a conversion of –20 × ΔSAOD (Section 7.3.4.6), or ERF = –20 × SAOD + 0.2582 W m^{-2} using absolute SAOD where SAOD is nominally taken at 550 nm wavelength. The SAOD conversion to ERF is expressed as an anomaly in SAOD relative to the 500 BCE to 1749 CE mean, so that the mean volcanic ERF for 500 BCE to 1749 CE is zero. This is in order that the long-term mean GSAT change from pre-industrial volcanic forcing alone is zero, avoiding a spurious cooling effect when applying the volcanic

time series from 1750 onwards to projections in a climate emulator (e.g. Section 7.SM.2). This convention means that volcanically quiescent years experience a volcanic ERF of up to +0.2 W m^{-2} (even volcanically quiescent years have some level of background stratospheric aerosol, so volcanic ERFs approaching the offset value of +0.2582 W m^{-2} are not seen). CMIP6 uses a similar prescription for volcanic forcing in ESMs, by applying a constant background climatology of SOAD for *piControl* and *ScenarioMIP* runs that is based on the historical (1850–2014) mean SAOD (Eyring et al., 2016).

The SAOD time series is derived from a composite of three datasets: eVolv v3 (Toohey and Sigl, 2017) for 500 BCE to 1900 CE, CMIP6 for 1850 to 1989, and GloSSAC v2 (Kovilakam et al., 2020) from 1979 to 2018. SAOD from GloSSAC v2 is reported at a wavelength of 525 nm and has been converted to 550 nm using an Ångström exponent of –2.33 (Kovilakam et al., 2020). The 2018 volcanic ERF is repeated for 2019. The 1850 to 1900 overlap is performed by linearly ramping down the eVolv v3 dataset and linearly ramping up the CMIP6 dataset. The CMIP6 and GloSSAC v2 data are ramped over the 1979 to 1989 period. In both cases the correspondences between overlapping periods is good.

Solar ERF is calculated using the change in total solar irradiance (TSI) where TSI is taken from the ^{14}C SATIRE-M reconstruction from PMIP4 (Jungclaus et al., 2017) and converted to ERF using ¼ × 0.71 × 0.72 × ΔTSI (Section 7.3.4.4). The baseline for TSI is the mean TSI from 6754 BCE to 1744 CE, which encompasses complete solar cycles in the proxy reconstructions before 1750.

Aerosols and solar ERFs in 2019 both differ from the headline assessments given in Sections 7.3.3 and 7.3.4.4 respectively. For aerosols, the assessment in Section 7.3.3 of –1.3 ± 0.7 W m^{-2} is valid for 1750 to about 2014, as less evidence is available for trends in how aerosol forcing has evolved in more recent years. The emissions-based time series provides a best-estimate aerosol ERF for 1750–2019 of –1.06 W m^{-2}, less negative than the 1750–2014 assessment, owing to a recent decline in precursor emissions since around 2005 from the CEDS dataset and supported by other studies (Paulot et al., 2018; Kanaya et al., 2020). For solar ERF, the Chapter 7 assessment of +0.01 ± 0.07 W m^{-2} is for the 6754 BCE to 1744 CE pre-industrial period to the 2009–2019 solar cycle. The single year 2019, corresponding to a solar minimum, has a solar ERF of –0.02 W m^{-2} relative to this pre-industrial baseline.

7.SM.1.3.2 Uncertainties in the historical best estimate time series

The uncertainty in the historical ERF time series was generated with a 100,000-member Monte Carlo ensemble. The forcing components where uncertainty ranges are assumed to be symmetric and Gaussian in their assessments in Section 7.3 have a scale factor drawn from a Gaussian distribution with mean of unity and 5–95% uncertainty range determined as a fraction of the best estimate ERF. The forcing components with symmetric uncertainty ranges are CO_2 (fractional 5–95% uncertainty 0.12 of the best estimate), CH_4 (0.20), N_2O (0.16), halogenated gases (0.19 on the basis that the majority are "long-lived"), ozone (0.50), stratospheric water vapour (1.00), land use change (0.50) and volcanic (0.25). Contrails (and aviation-induced cirrus) and light-absorbing particles on snow and ice have asymmetric uncertainty ranges and the fractional uncertainty was determined by considering ranges below and above the best estimate separately, by dividing the 5th percentile by the best estimate to derive the lower uncertainty range and the 95th percentile by the best estimate to determine the upper range, treating them as two halves of a Gaussian distribution. In each ensemble member the sampled uncertainty scale factor for each component of the forcing is applied to the whole time series.

For aerosols, the ERFari and ERFaci are treated independently. ERFari uncertainty is developed by sampling the radiative efficiency coefficients β_{BC}, β_{OC}, β_{SO2} and β_{NH3} in Eq. (7.SM.1.1) as Gaussian distributions with 5–95% ranges uncertainties of 0.67, 0.78, 0.50 and 0.44, yielding contributions to ERFari of +0.3 ± 0.2 W m^{-2} for BC, –0.4 ± 0.2 W m^{-2} for sulphate, –0.09 ± 0.07 W m^{-2} for OC and –0.11 ± 0.05 W m^{-2} for nitrate for the 2005–2014 mean with respect to 1750. Each precursor species is sampled independently and the historical emissions from the CEDS database are used to generate the time series of ERFari. For ERFaci, the 100,000 generated time series described in Section 7.SM.1.3 are used with one additional step to scale each ERFaci candidate time series to a 2005–2014 mean ERFaci of –1.0 ± 0.7 W m^{-2} with respect to 1750. This

effectively rescales the β coefficients in each ensemble member in Eq. (7.SM.1.2) .

The 5–95% range of anthropogenic ERF of 1.96–3.48 W m^{-2} (Table 7.8) for 1750–2019 is determined from the 5th and 95th percentiles of the year 2019 anthropogenic ERF in this 100,000 member ensemble.

For solar forcing, a 0.50 fractional uncertainty was applied to the amplitude of the solar cycle, and a linear 1750 to 2019 trend of ±0.07 W m^{-2} (5–95%) range was added to this to represent the uncertainty in the change in the underlying solar forcing (Section 7.3.4.4).

7.SM.1.4 SSP and RCP effective radiative forcing time series

A similar method to the process described in Section 7.SM.1.3 is used to derive the ERF time series in RCP and SSP scenarios to 2500 (Annex III; Figure 4.36; Chapter 6; Chapter 9). From 1750 to 2014 the best estimate and uncertainty SSP projections ERF time series and the historical ERF time series described are identical. The SSPs diverge from each other, and from the historical best estimate, in 2015. For SSPs, the set of eight Tier 1 and Tier 2 scenarios defined by *ScenarioMIP* are assessed (SSP1-1.9, SSP1-2.6, SSP4-3.4, SSP5-3.4-over, SSP2-4.5, SSP4-6.0, SSP3-7.0 and SSP5-8.5). In addition two variants of SSP3-7.0 used primarily by AerChemMIP are presented: one where short-lived climate forcers are set to emissions factors consistent with strong air-quality controls that are broadly consistent with SSP1-levels of mitigation, SSP3-7.0-lowNTCF (Collins et al., 2017), plus a further variant of SSP3-7.0-lowNTCF that also takes into account methane mitigation alongside other short-lived forcers, SSP3-7.0-lowNTCFCH4 (Allen et al., 2021).

For 2015 to 2020, a linear transition between the concentrations of well-mixed greenhouse gases provided by Chapter 2 and the SSP greenhouse gas concentrations from Meinshausen et al. (2020) is performed. From 2020 onwards concentration projections from Meinshausen et al. (2020) are used. The correspondence between the Chapter 2 assessed time series and Meinshausen et al. (2017) dataset used for the CMIP6 *historical* experiment is good, with a maximum difference of 0.6% from 1850-2014 for the main three greenhouse gases and 1.4% for N_2O in 1750 (the slight 1750 concentration differences affects the $2\times CO_2$ forcing in the third decimal place; see Table 7.SM.2).

For purely emissions-based forcing estimates (aerosols, contrails and aviation-induced cirrus, and black carbon on snow), a similar 5-year transition between 2015 and 2020 is performed for fossil fuel, industrial and agricultural emissions. The best-estimate historical emissions to 2019 are provided in the 11 September 2020 version of the CEDS database (https://doi.org/10.5281/zenodo.4025316) and the SSP scenario projections used v5.1 of the RCMIP dataset (obtained from https://doi.org/10.5281/zenodo.4589756; Nicholls et al., (2020)) that provides consolidated regional and sectoral annual emissions totals from the CMIP6 SSP emissions datasets (Velders et al., 2015; Gidden et al., 2019; Meinshausen et al., 2020). Biomass burning emissions are used from the SSP emissions projections from Van Marle et al. (2017). The same parameter sets from the historical ERF estimate and 100,000 member Monte Carlo ensemble are used to derive the future ERFs from aerosols, contrails (and aviation-induced cirrus) and black carbon on snow, using the SSP emissions projections.

Future ozone forcing for SSP projections differs from the historical treatment and is based on emissions of short-lived forcers and concentrations of ozone-depleting greenhouse gases (Section 6.4). To generate the best-estimate projection, the historical time series in Skeie et al. (2020) is matched to emissions-driven estimates of ozone ERF from AerChemMIP models (Thornhill et al., 2021b), displayed in Table 7.SM.3 that sums to +0.37 W m^{-2} for 1850 to 2014. There is a temperature-dependent feedback on ozone ERF of –0.037 W m^{-2} °C^{-1} for CMIP historical runs (this differs from the assessment in Section 6.4 of –0.064 W m^{-2} °C^{-1} which is based on *abrupt4xCO2* experiments, as it includes the effects of the lightning NOx and BVOC feedbacks that act to reduce the magnitude of the temperature-ozone feedback (Thornhill et al., 2021a)). As five of the six Earth System Models run in Skeie et al. (2020) considered in the ERF ozone assessment were CMIP historical runs (all except Oslo-CTM3) and simulated the increase in historical GSAT over time, they implicitly included this feedback and as such the –0.037 W m^{-2} °C^{-1} feedback it is subtracted from the transient ozone ERF in these five models, using GSAT time series assessed in Chapter 2, to produce a "zero-

feedback" estimate of ozone forcing from 1850 to 2014 of +0.47 W m^{-2}. To apply the emissions precursors to the overall time series, they are scaled by a factor of 1.27, derived from a ratio of the zero feedback estimate from Skeie et al. (2020) to the best estimate from the sum of precursors from Thornhill et al. (2021b) (0.47/0.37) to produce radiative efficiencies for each species (Table 7.SM.3).

[START TABLE 7.SM.3 HERE]

Table 7.SM.3: ERF from ozone precursors in AerChemMIP experiments (Thornhill et al., 2021b), and radiative efficiencies derived for emissions-based SSP pathways. The contributions for CO + NMVOC are not separated in Thornhill et al. (2021b) so the ratio of CO : NMVOC from CMIP5 ACCMIP experiments is used (Stevenson et al., 2013). "Concentrations" of ozone-depleting halocarbons (ODHs) are expressed in equivalent effective stratospheric chlorine in ppt.

species	Contribution to ozone ERF 1850-2014, W m^{-2} (Stevenson et al., 2013; Thornhill et al., 2021b)	Scale factor to reproduce 1850-2014 ozone ERF in Skeie et al. (2020), after subtracting temperature feedback	Radiative efficiency for ozone ERF
CH_4	+0.14 ± 0.05	1.27	β_{CH4} = 0.175 ± 0.062 mW m^{-2} ppb^{-1}
N_2O	+0.03 ± 0.02		β_{N2O} = 0.710 ± 0.062 mW m^{-2} ppb^{-1}
Ozone-depleting halocarbons (ODH)	–0.11 ± 0.10		β_{ODH} = –0.125 ± 0.113 mW m^{-2} ppt^{-1}
CO	+0.07 ± 0.06		β_{CO} = 0.155 ± 0.131 mW m^{-2} $MtCO^{-1}$ yr
NMVOC	+0.04 ± 0.04		β_{NMVOC} = 0.329 ± 0.328 mW m^{-2} $MtNMVOC^{-1}$ yr
NOx	+0.20 ± 0.11		β_{NOx} = 1.797 ± 0.983 mW m^{-2} $MtNO_2$ yr^{-1}
Sum	+0.37 ± 0.18	+0.47 ± 0.24 W m^{-2} (total ozone ERF)	

[END TABLE 7.SM.3 HERE]

The future ozone ERF is then derived as

$$ERF_{O3} = \beta_{CH4}\Delta C_{CH4} + \beta_{N2O}\Delta C_{N2O} + \beta_{ODH}\Delta C_{ODH} + \beta_{CO}\Delta E_{CO} + \beta_{NMVOC}\Delta E_{NMVOC} + \beta_{NOx}\Delta E_{NOx} - f \cdot \Delta T \quad \textit{Equation 7.SM.1.3}$$

where C_{CH4} and C_{N2O} are concentrations of CH_4 and N_2O in ppb, C_{ODH} is the equivalent effective stratospheric chlorine from halogenated compounds expressed in ppt (Newman et al., 2007), and E_{CO}, E_{NMVOC} and E_{NOx} are annual emissions in Mt yr^{-1} (NOx expressed in units of $MtNO_2$), f = –0.037 W m^{-2} $°C^{-1}$ and ΔT represents GSAT anomaly. This configuration is run iteratively, with other best-estimate forcings, in the two-layer emulator (Section 7.SM.2) with the Section 7.5.5 best-estimate assessments of equilibrium climate sensitivity (ECS, 3.0°C) and transient climate response (TCR, 1.8°C) until convergence is achieved.

ERF from land use change scales with cumulative emissions of land-use-related CO_2 emissions following the end of the historical period.

Volcanic forcing is set to a ten-year linear ramp down to zero from 2014 to 2024, following the CMIP6 ScenarioMIP protocol (Eyring et al., 2016). Solar forcing uses the CMIP6 future TSI variation (Matthes et al., 2017) which provides projections to 2299, and is set to zero from 2300. For Figure 4.36 and Annex III, ERF time series for the RCP scenarios are produced using emissions and concentrations from Meinshausen et al. (2011b) using the same methods, present-day forcing best estimates, and uncertainty ranges described above, with the difference that scenarios start to diverge in 2005 and a 15-year ramp from 2005 to 2020 from historical emissions or concentrations to the future RCP projections is performed.

[START FIGURE 7.SM.1 HERE]

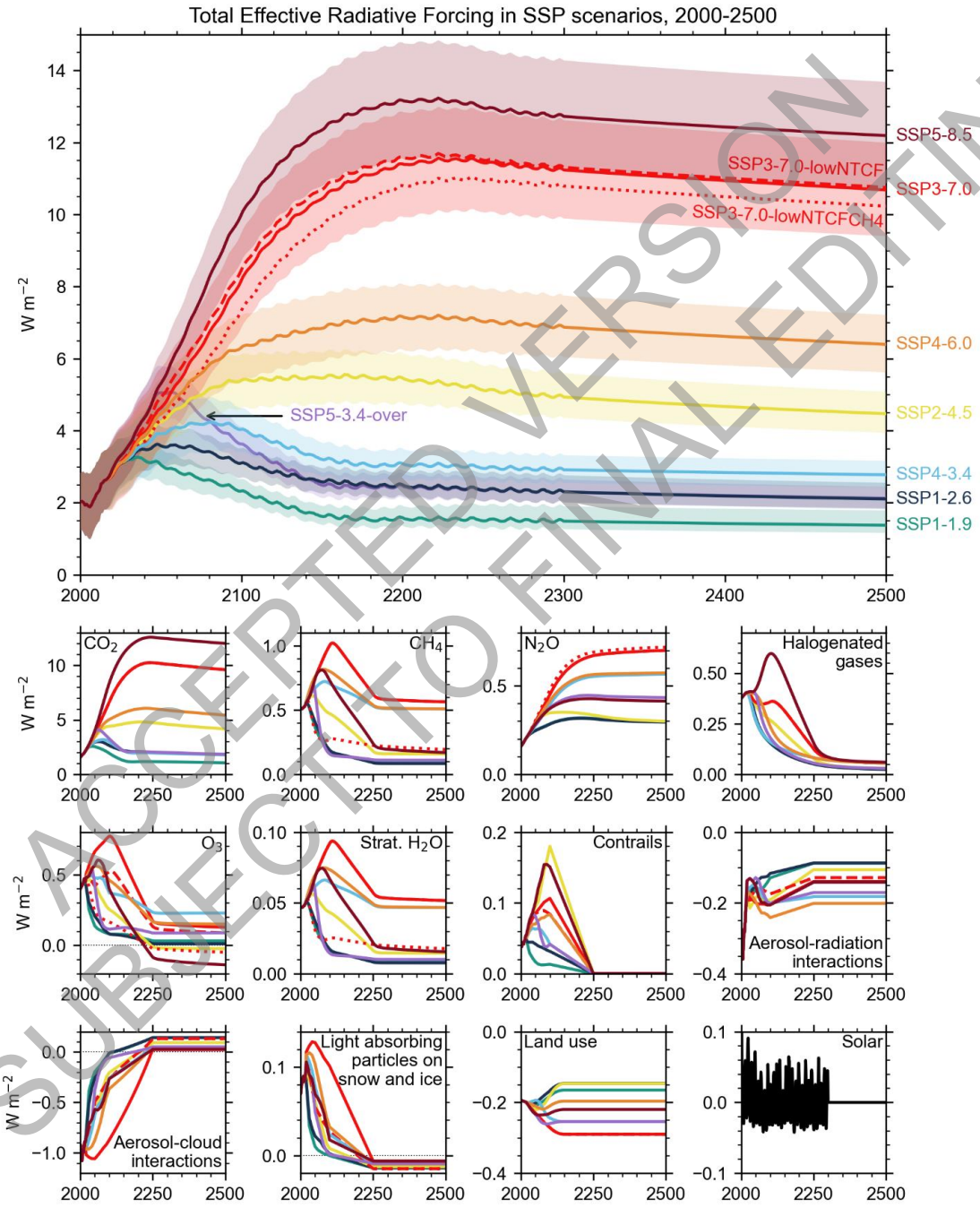

Figure 7.SM.1: Total effective radiative forcing from SSP scenarios with respect to 1750 for 2000-2500 (top panel), showing best estimate and 5–95% uncertainty range (shaded regions). Uncertainty ranges are not shown for SSP3-7.0-lowNTCF and SSP3-7.0-NTCFCH4 for visual clarity. Bottom matrix shows the

best estimate ERF for each anthropogenic component, and solar (volcanic ERF is zero beyond 2024).
[END FIGURE 7.SM.1 HERE]

7.SM.2 Two-layer energy balance model for climate emulation

7.SM.2.1 Emulator definition

The two-layer emulator is based on the following global mean equations:

$$C\frac{\mathrm{d}}{\mathrm{d}t}\Delta T = \Delta F(t) + \alpha\Delta T - \varepsilon\gamma(\Delta T - \Delta T_d)$$
$$C_\mathrm{d}\frac{\mathrm{d}}{\mathrm{d}t}\Delta T_\mathrm{d} = \gamma(\Delta T - \Delta T_d) \qquad \textit{Equation 7.SM.2.1}$$

where ΔT (°C) is the temperature of the surface layer (representing the surface components of the climate system), ΔT_d (°C) is the temperature change in the deep ocean layer, C and C_d are the effective heat capacities for the surface and deep layers in W yr m^{-2} °C^{-1}, ε is the efficacy of the deep ocean heat uptake and γ is the heat transfer coefficient between the surface and deep layer (W m^{-2} °C^{-1}).

The analytical solution of Eq. (7.SM.2.1) is expressed by a combination of fast and slow modes with the decay time scales of τ_f and τ_s. For a given value of ECS, TCR is obtained as

$$\mathrm{TCR} = \mathrm{ECS}\left\{1 - \frac{1}{t}\left[\tau_f a_f\left(1 - e^{-\frac{t_0}{\tau_f}}\right) - \tau_s a_s\left(1 - e^{-\frac{t_0}{\tau_s}}\right)\right]\right\}. \qquad \textit{Equation 7.SM.2.2}$$

The TCR is equal to ΔT at year $t = t_0 = 70$ in response to the forcing ΔF increasing at a rate of 1% per year, and all parameters (τ_f, τ_s, a_f, and a_s) can be calculated using C, C_d, γ, ε and the net feedback parameter α (the formulae are presented in Geoffroy et al. (2013a)). As discussed in Jiménez-de-la-Cuesta and Mauritsen (2019), TCR can also be estimated directly from the two-layer model parameters as $\mathrm{TCR} = \Delta F_{2\times\mathrm{CO2}}/(-\alpha + \kappa)$, where $\kappa = \varepsilon\gamma$.

The two-layer model can be calibrated to emulate the climate response of individual CMIP models (Geoffroy et al., 2013b, 2013a) using *abrupt4xCO2* experiments. Calibrations are performed for 44 CMIP6 models resulting in parameter estimates (mean and standard deviation) of C = 8.1 ± 1.0 W yr m^{-2} °C^{-1}, C_d = 110 ± 63 W yr m^{-2} °C^{-1}, γ = 0.62 ± 0.13 W m^{-2} °C^{-1}, ε = 1.34 ± 0.41, κ = 0.84 ± 0.38 W m^{-2} °C^{-1}. Representative values from CMIP6 models in Eq. (7.SM.2.2) are τ_f = 4.6 yr, τ_s = 333 yr, a_f = 0.541, a_s = 0.459.

7.SM.2.2 Constrained emulator ensemble

In several places in Working Group I (Chapter 1, Figure 7.7, Figure 7.8, Chapter 9), a constrained ensemble of two-layer model projections is used. The starting point for this ensemble is a 1 million-member ensemble of emissions-driven historical runs using v1.6.2 of the FaIR emulator (Millar et al., 2017; Smith et al., 2018a). The temperature module of FaIR is mathematically equivalent to the two-layer emulator in Eq. (7.SM.2.1), and the emissions- or concentrations-to-ERF relationships in FaIR are equivalent or very similar to those described in generating the ERF time series in Section 7.SM.1. The similarity of the two-layer model to FaIR is demonstrated in Figure 7.SM.2.

The 1 million ensemble members sample the uncertainty in the ERF, the climate response, and the carbon cycle. ERF uncertainties are generated using the same method described in Section 7.SM.1.3. For the climate response, the C, C_d, γ and ε components of the two-layer model in Eq. 7.SM.2.1 are generated from kernel-

density estimates that are calibrated to 44 CMIP6 models (Section 7.SM.2.1). The climate feedback parameter α is sampled from a truncated Gaussian distribution (truncated at ±2 standard deviations) with mean –1.33 W m^{-2} °C^{-1} and standard deviation 0.5 W m^{-2} °C^{-1}. The carbon cycle in FaIR is parameterised by the pre-industrial time-integrated airborne fraction of CO_2, and the change in airborne fraction with accumulated carbon emissions and GSAT change (Millar et al., 2017). These parameters are sampled as uniform distributions using the lowest and highest values based on calibrations to 11 CMIP6 models (Arora et al., 2020) as the bounds of the distributions. The 1 million-member ensemble was run in the FaIR model using emissions-driven runs from 1750 to 2019. The resulting ensemble was constrained based on agreement to:

(1) the time series of historical GSAT to the Chapter 2 (Cross Chapter Box 2.3) assessment from 1850–2020 with a root-mean-square error of 0.135°C or less, approximately recreating the headline 1850–1900 to 1995–2014 assessment of 0.67–0.98°C (Cross Chapter Box 2.3, *very likely* range);
(2) the assessment of ocean heat uptake from Section 7.2.2.2 from 1971–2018 within the *likely* range of 329–463 ZJ;
(3) CO_2 concentrations to the 2014 *very likely* range of 397.1 ± 0.4 ppm (Table 2.1);
(4) the airborne fraction from a 1% per year CO_2 increase simulation to the range assessed in Section 5.5.1 of 53 ± 6% (1 standard deviation).

From the original 1 million-member ensemble, 2,237 ensemble members passed all four constraints and are used for reporting results. This constrained ensemble set from FaIRv1.6.2 has a good correspondence to assessed ranges of key climate metrics across the Working Group I report (Cross Chapter Box 7.1 Table 1; Table 7.SM.4). While not used as formal constraints, the assessed distributions of ECS and TCR (Section 7.5.2) and projected future warming from the five major SSP scenarios (Section 4.3.4) were used as guidelines to ensure simultaneous adherence to several assessed ranges. As a comparison, the ECS from this constrained set has a median and 5–95% ranges of ECS and TCR of 2.95 [2.05 – 5.07]°C and 1.81 [1.36–2.46]°C respectively, compared to the Chapter 7 best estimates and *very likely* ranges of 3.0 [2.0–5.0]°C for ECS and 1.8 [1.2 – 2.4]°C for TCR. While constraints (3) and (4) are not required when running FaIR or the two-layer model using prescribed historical greenhouse gas concentrations, this 2,237 member ensemble set is intended to be used to evaluate future warming pathways to integrated assessment model scenario projections in Chapter 3 of Working Group III, so the same ensemble set is used here for overall consistency.

7.SM.2.3 Supporting information for Figures 7.7 and 7.8

The data contributing to Figures 7.7 and 7.8 is from the 2,237-member constrained ensemble described in Section 7.SM.2.2. To provide the contributions to historical temperature in Figures 7.7 and 7.8, one of the 13 components of the historical forcing at a time is removed from the total forcing, and the two-layer model run using the forcing and climate configuration from each of the 2,237 ensemble members. The difference between the all-forcing and leave-one-out model run provides the temperature contribution from each forcing agent. This exercise was repeated using a best-estimate climate response (hence, only assessing the impact of uncertainty in the ERF) by setting ECS = 3.0°C, TCR 1.8°C and the other two-layer model parameters set to their CMIP6 model means (C = 8.1 W yr m^{-2} °C^{-1}, C_d = 110 W yr m^{-2} °C^{-1}, γ = 0.64 W m^{-2} °C^{-1} and ε = 1.36; Section 7.SM.2.1). These simulations are shown as dashed error bars in Figure 7.7, with the full ERF and climate response uncertainty as solid error bars.

Each ensemble member uses a long (approximately 9,000-year) pre-industrial spin-up comprising only transient solar and volcanic forcing starting in 6755 BCE (Section 7.SM.1.3), and temperature changes are reported with respect to 1750 as a single baseline year. The same 2,237 ensemble member set was extended forward in time to 2500 under forcing from the SSP scenarios (Section 7.SM.1.4) and used to inform global-mean sea level projections in Chapter 9.

7.SM.3 Performance of emulators compared to key physical climate assessments

Table 7.SM.4 details the performance of the four emulators (CICERO-SCM, FaIRv1.6.2, MAGICC7.5.1 and OSCARv3.1.1) described in Cross Chapter Box 7.1 for a number of climate assessments in absolute terms, and can be compared to Cross Chapter Box 7.1 Table 2 which details the relative difference between each emulator and the AR6 assessed range.

[START TABLE 7.SM.4 HERE]

Table 7.SM.4: Absolute differences between the emulator value and the Working Group I assessed best estimate and range for key climate assessments. Values are given for four emulators in their respective AR6-calibrated probabilistic setups. Relative values of these indicators are shown in Cross Chapter Box 7.1, Table 2. Emulator values within 5% of the assessed central value and 10% of the lower and upper ranges are unshaded, showing good correspondence between the emulator and the assessment. The columns labelled "upper" and "lower" indicate *very likely* (5% to 95%) ranges, except for the variables demarcated with an asterisk or double asterisk (* or **), where they denote *likely* ranges from 17% to 83%. Note that the TCRE assessed range (**) is wider than the combination of the TCR and airborne fraction to account for uncertainties related to model limitations.

Emulator		Assessed ranges			CICERO-SCM			FaIRv1.6.2			MAGICC7			OSCARv3.1.1		
Assessed range		**Lower**	**Central**	**Upper**	**Lower**	**Central**	**Upper**	**Lower**	**Central**	**Upper**	**Lower**	**Central**	**Upper**	**Lower**	**Central**	**Upper**
Key metrics																
ECS (°C)		2.00	3.00			3.05	4.09	2.05	2.95	5.07	1.93	2.97	4.83	1.84	2.54	3.90
TCRE (°C per 1000 GtC)**		1.00	1.65	2.30				1.29	1.53	1.82	1.37	1.73	2.19	1.50	1.52	1.83
TCR (°C)		1.20	1.80	2.40	1.38	1.71	2.32	1.36	1.81	2.46	1.27	1.88	2.61	1.51	1.82	2.05
Historical warming and Effective Radiative Forcing																
GSAT warming (°C)	1995-2014 relative to 1850-1900	0.67	0.85	0.98	0.68	0.85	0.98	0.72	0.87	1.02	0.72	0.86	0.97	0.67	0.78	0.98
Ocean heat content change (ZJ)*	1971-2018	329	396	463	250	288	329	346	381	423	325	382	436	174	243	508

Total Aerosol ERF (W m^{-2})	2005-2014 relative to 1750	-2.00	-1.30	-0.60	-1.27	-0.82	-0.54	-1.68	-1.15	-0.60	-1.79	-1.20	-0.55	-1.24	-1.11	-0.79
WMGHG ERF (W m^{-2})	2019 relative to 1750	3.03	3.32	3.61	3.14	3.14	3.14	3.07	3.38	3.66	3.10	3.35	3.60	3.06	3.42	3.49
Methane ERF (W m^{-2})	2019 rel. 1750	0.43	0.54	0.65	0.56	0.56	0.56	0.44	0.56	0.67	0.43	0.54	0.67	0.47	0.54	0.62
Carbon Cycle metrics																
Airborne Fraction 1pctCO2 (dimensionless)*	2×CO_2	0.47	0.53	0.59				0.50	0.52	0.53	0.52	0.56	0.59	0.47	0.53	0.64
Airborne Fraction 1pctCO2 (dimensionless)*	4×CO_2	0.50	0.60	0.70				0.56	0.60	0.63	0.57	0.62	0.66	0.53	0.59	0.69
Future warming (GSAT) relative to 1995-2014																
SSP1-1.9 (°C)	2021-2040	0.38	0.61	0.85	0.42	0.58	0.94	0.39	0.61	0.94	0.39	0.61	0.88	0.43	0.55	0.64
	2041-2060	0.40	0.71	1.07	0.43	0.65	1.15	0.36	0.66	1.14	0.39	0.71	1.15	0.45	0.65	0.74
	2081-2100	0.24	0.56	0.96	0.21	0.42	0.94	0.18	0.48	1.00	0.20	0.52	0.99	0.26	0.51	0.66
SSP1-2.6 (°C)	2021-2040	0.41	0.63	0.89	0.44	0.60	0.94	0.42	0.64	0.96	0.40	0.62	0.89	0.45	0.57	0.64
	2041-2060	0.54	0.88	1.32	0.58	0.83	1.34	0.53	0.86	1.38	0.54	0.89	1.35	0.62	0.82	0.95
	2081-2100	0.51	0.90	1.48	0.50	0.78	1.41	0.47	0.84	1.49	0.48	0.89	1.49	0.59	0.82	1.05

SSP2-4.5 (°C)	2021-2040	0.44	0.66	0.90	0.48	0.63	0.94	0.47	0.65	0.92	0.45	0.64	0.89	0.42	0.57	0.63
	2041-2060	0.78	1.12	1.57	0.81	1.08	1.62	0.79	1.11	1.59	0.79	1.13	1.60	0.84	1.03	1.12
	2081-2100	1.24	1.81	2.59	1.22	1.63	2.51	1.21	1.75	2.63	1.21	1.82	2.67	1.34	1.74	1.96
SSP3-7.0 (°C)	2021-2040	0.45	0.67	0.92	0.50	0.64	0.93	0.51	0.68	0.91	0.49	0.68	0.92	0.43	0.57	0.65
	2041-2060	0.92	1.28	1.75	0.96	1.22	1.74	0.98	1.28	1.72	0.98	1.33	1.77	0.99	1.17	1.29
	2081-2100	2.00	2.76	3.75	1.99	2.55	3.64	2.07	2.72	3.72	2.13	2.86	3.97	2.09	2.59	2.81
SSP5-8.5 (°C)	2021-2040	0.51	0.76	1.04	0.54	0.71	1.06	0.56	0.77	1.08	0.55	0.77	1.06	0.51	0.66	0.73
	2041-2060	1.08	1.54	2.08	1.11	1.42	2.07	1.12	1.55	2.17	1.11	1.57	2.16	1.19	1.44	1.58
	2081-2100	2.44	3.50	4.82	2.54	3.24	4.68	2.58	3.50	4.89	2.63	3.65	5.16	2.65	3.35	3.62

[START TABLE 7.SM.4 HERE]

The comparison of the constrained two-layer emulator to FaIRv1.6.2 and MAGICC7.5.1 is shown in Figure 7.SM.3 for the SSP1-2.6 and SSP5-8.5 scenarios, demonstrating the similarity between the FaIR and two-layer projections as well as the similarity between FaIR and MAGICC in their AR6 setups.

[START FIGURE 7.SM.2 HERE]

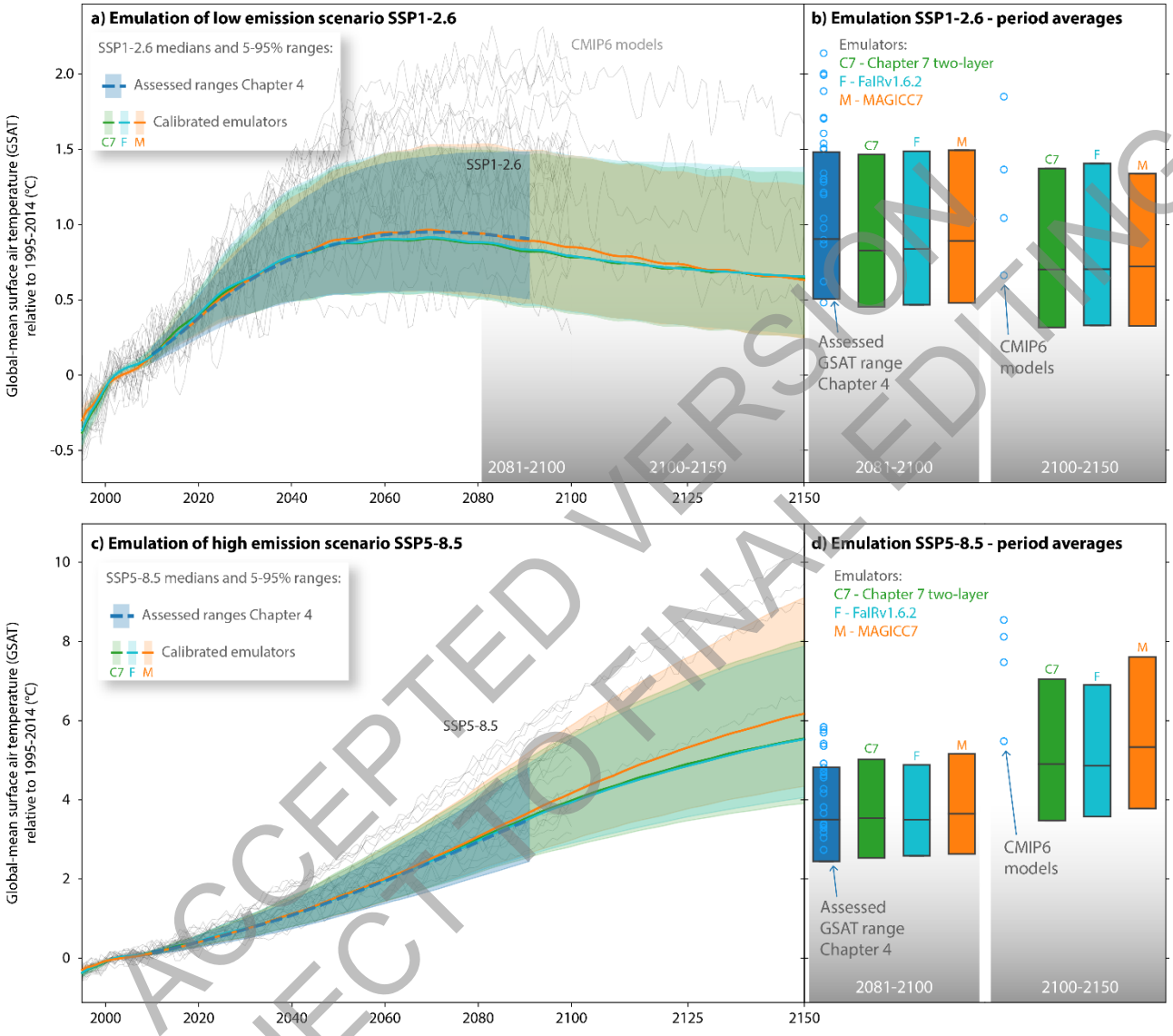

Figure 7.SM.2: (a) Time series and (b) 2100-2150 means of emulated GSAT projections from the Chapter 7 two-layer model (green), FAIRv1.6.2 (light blue), and MAGICC7.5.1 (orange) from 1995 to 2150, following the SSP1-2.6 scenario ((a) and (b)) and the SSP5-8.5 scenario ((c) and (d)). In (a) and (c) the ensemble median estimates are solid lines and the 5–95% ranges are shaded; in (b) and (d) the bar range shows 5–95% ranges with the median in black. Overlaid CMIP6 model results are shown as lines in (a) and (c), and dots in (b) and (d) (fewer dots are shown for the 2100–2150 period because only a limited number of CMIP6 models have performed runs beyond 2100). In (a) and (c), Chapter 4 assessed GSAT projections (20-year running means) are shown with a dark blue dashed line and 5-95% range in dark blue shading.

[END FIGURE 7.SM.2 HERE]

7.SM.4 Equilibrium Climate Sensitivity and Transient Climate Response from CMIP6 models

Table 7.SM.5 details the equilibrium climate sensitivity and transient climate response estimated from CMIP6 and CMIP5 models using the ESMValTool (Eyring et al., 2020; Lauer et al., 2020; Righi et al., 2020) and presented in Schlund et al. (2020) for ECS and Meehl et al. (2020) for TCR (CMIP6 only), used in Section 7.5.6, Figure 7.18 and FAQ 7.3. Climate feedback parameters, including the decomposition into Planck, water vapour plus lapse rate, surface albedo and cloud components, plus the residual, are given for CMIP6 and CMIP5 models from Zelinka et al. (2020). ECS is estimated from a 150-year integration of an *abrupt4xCO2* experiment, subtracting the parallel *piControl* integration from the same period, regressing the modelled top-of-atmosphere energy imbalance ΔN against the modelled GSAT change ΔT, and taking $\Delta T/2$ at the point where the regression slope crosses $\Delta N = 0$ (Gregory et al., 2004). TCR is estimated from the mean ΔT change from a *1pctCO2* run compared to the parallel *piControl* integration in years 60 to 79. Feedback contributions are estimated from a mean of six radiative kernels presented in Zelinka et al. (2020).

[START TABLE 7.SM.5 HERE]

Table 7.SM.5: Equilibrium climate sensitivity (ECS) and climate feedbacks estimated from CMIP5 and CMIP6 models. Transient climate response (TCR) from CMIP6 models is also provided. Data from Schlund et al. (2020), Meehl et al. (2020) and Zelinka et al. (2020).

MIP Era	Model	ECS °C	Net feedback α, W m^{-2} °C^{-1}	Components of the net feedback, W m^{-2} °C^{-1}					TCR °C
				Planck	Water vapour + lapse rate	Surface albedo	Cloud	Residual	
CMIP6	ACCESS-CM2	4.72	–0.74	–3.22	1.18	0.37	0.80	0.14	2.10
	ACCESS-ESM1-5	3.87	–0.73	–3.21	1.33	0.42	0.62	0.11	1.95
	AWI-CM-1-1-MR	3.16	–1.15	–3.16	1.27	0.42	0.29	0.04	2.06
	BCC-CSM2-MR	3.04	–1.03	–3.25	1.23	0.38	0.57	0.04	1.72
	BCC-ESM1	3.26	–0.92	–3.23	1.24	0.42	0.58	0.06	1.77
	CAMS-CSM1-0	2.29	–1.82	–3.25	1.30	0.24	-0.30	0.20	1.73
	CAS-ESM2-0	3.51							2.04
	CESM2	5.16	–0.63	–3.28	1.26	0.38	1.01	-0.01	2.06
	CESM2-FV2	5.14	–0.55	–3.23	1.17	0.40	1.10	0.01	2.05
	CESM2-WACCM	4.75	–0.71	–3.27	1.25	0.37	1.22	-0.28	1.98
	CESM2-WACCM-FV2	4.79	–0.61	–3.24	1.16	0.37	1.17	-0.07	2.01
	CIESM		–0.69	–3.19	1.19	0.27	0.84	0.20	2.39
	CMCC-CM2-SR5	3.52	–1.07	–3.26	1.27	0.31	0.58	0.04	2.09
	CMCC-ESM2		–1.05	–3.25	1.29	0.33	0.56	0.02	
	CNRM-CM6-1	4.83	–0.74	–3.22	1.24	0.49	0.61	0.14	2.14
	CNRM-CM6-1-HR	4.28	–0.92	–3.27	1.27	0.37	0.59	0.13	2.48
	CNRM-ESM2-1	4.76	–0.62	–3.23	1.27	0.47	0.63	0.25	1.86
	CanESM5	5.62	–0.65	–3.26	1.29	0.42	0.88	0.03	2.74
	E3SM-1-0	5.32	–0.63	–3.27	1.25	0.32	0.97	0.11	2.99

	EC-Earth3		–0.76	–3.18	1.45	0.53	0.39	0.05	2.30
	EC-Earth3-AerChem		–0.94	–3.18	1.39	0.54	0.27	0.05	
	EC-Earth3-Veg	4.31	–0.78	–3.21	1.45	0.53	0.37	0.07	2.62
	FGOALS-f3-L	3.00	–1.40	–3.14	1.21	0.36	0.04	0.13	1.94
	FGOALS-g3	2.88	–1.25	–3.23	1.45	0.49	0.10	-0.06	1.54
	FIO-ESM-2-0								2.22
	GFDL-CM4		–0.82	–3.18	1.23	0.50	0.64	-0.01	
	GFDL-ESM4		–1.42	–3.25	1.18	0.34	0.50	-0.19	
	GISS-E2-1-G	2.72	–1.46	–3.20	1.06	0.24	0.07	0.38	1.80
	GISS-E2-1-H	3.11	–1.13	–3.16	1.27	0.42	0.06	0.28	1.93
	GISS-E2-2-G		–1.51	–3.19	1.18	0.32	0.01	0.18	1.71
	HadGEM3-GC31-LL	5.55	–0.63	–3.21	1.19	0.38	0.84	0.17	2.55
	HadGEM3-GC31-MM	5.42	–0.66	–3.23	1.18	0.32	0.91	0.16	2.58
	IITM-ESM		–1.91	–3.22	1.16	0.26	-0.02	-0.08	1.71
	INM-CM4-8	1.83	–1.48	–3.23	1.45	0.36	-0.09	0.02	1.33
	INM-CM5-0	1.92	–1.52	–3.23	1.40	0.40	-0.06	-0.03	
	IPSL-CM5A2-INCA		–0.81	–3.25	1.23	0.33	1.05	-0.16	
	IPSL-CM6A-LR	4.56	–0.76	–3.22	1.35	0.44	0.45	0.22	2.32
	KACE-1-0-G	4.48	–0.72	–3.24	1.17	0.33	0.84	0.18	1.41
	MCM-UA-1-0	3.65							1.94
	MIROC-ES2L	2.68	–1.54	–3.26	1.19	0.40	0.04	0.08	1.55
	MIROC6	2.61	–1.40	–3.29	1.30	0.47	0.22	-0.10	1.55
	MPI-ESM-1-2-HAM	2.96	–1.41	–3.10	1.18	0.36	-0.16	0.32	1.80
	MPI-ESM1-2-HR	2.98	–1.22	–3.14	1.21	0.38	0.27	0.05	1.66
	MPI-ESM1-2-LR	3.00	–1.39	–3.11	1.12	0.37	0.18	0.05	1.84
	MRI-ESM2-0	3.15	–1.10	–3.20	1.16	0.54	0.46	-0.06	1.64
	NESM3	4.72	–0.78	–3.09	1.19	0.50	0.45	0.17	2.72
	NorCPM1	3.05	–1.10	–3.17	1.31	0.44	0.30	0.01	1.56
	NorESM2-LM	2.54	–1.34	–3.30	1.28	0.35	0.44	-0.11	1.48
	NorESM2-MM	2.50	–1.50	–3.32	1.29	0.30	0.51	-0.28	1.33
	SAM0-UNICON	3.72	–1.04	–3.27	1.13	0.38	0.75	-0.03	2.27
	TaiESM1	4.31	–0.88	–3.25	1.26	0.40	0.70	0.00	2.34
	UKESM1-0-LL	5.34	–0.67	–3.19	1.19	0.48	0.87	-0.01	2.79
CMIP6 mean		3.78	–1.03	–3.22	1.25	0.39	0.49	0.05	2.01
CMIP6 standard deviation		1.08	0.36	0.05	0.09	0.08	0.38	0.14	0.41
CMIP5	ACCESS1-0	3.83	–0.76	–3.18	1.26	0.43	0.47	0.25	

	ACCESS1-3	3.53	–0.81	–3.21	1.25	0.41	0.65	0.08	
	BNU-ESM	3.92	–0.92	–3.14	1.35	0.61	0.20	0.05	
	CCSM4	2.94	–1.18	–3.19	1.28	0.48	0.27	-0.02	
	CNRM-CM5	3.25	–1.13	–3.20	1.24	0.46	0.15	0.21	
	CNRM-CM5-2	3.44							
	CSIRO-Mk3-6-0	4.08	–0.64	–3.26	1.25	0.38	0.67	0.32	
	CanESM2	3.69	–1.03	–3.28	1.35	0.39	0.52	-0.02	
	FGOALS-g2	3.38	–0.84	–3.18	1.40	0.59	0.38	-0.03	
	FGOALS-s2		–0.91	–3.19	1.32	0.52	0.03	0.42	
	GFDL-CM3	3.97	–0.76	–3.18	1.08	0.43	0.88	0.02	
	GFDL-ESM2G	2.39	–1.23	–3.20	1.17	0.30	0.22	0.27	
	GFDL-ESM2M	2.44	–1.37	–3.20	1.13	0.29	0.11	0.30	
	GISS-E2-H	2.31	–1.66	–3.16	1.27	0.32	-0.12	0.03	
	GISS-E2-R	2.11	–1.76	–3.17	1.30	0.24	-0.14	0.01	
	HadGEM2-ES	4.61	–0.63	–3.17	1.30	0.40	0.70	0.14	
	IPSL-CM5A-LR	4.13	–0.75	–3.26	1.20	0.27	1.18	-0.14	
	IPSL-CM5A-MR	4.12	–0.80	–3.28	1.18	0.19	1.25	-0.14	
	IPSL-CM5B-LR	2.60	–1.02	–3.17	1.32	0.28	0.62	-0.06	
	MIROC-ESM	4.67	–0.92	–3.32	1.23	0.50	0.68	-0.02	
	MIROC5	2.72	–1.53	–3.24	1.29	0.48	-0.04	-0.02	
	MPI-ESM-LR	3.63	–1.13	–3.16	1.09	0.44	0.44	0.06	
	MPI-ESM-MR	3.46	–1.19	–3.17	1.05	0.39	0.47	0.06	
	MPI-ESM-P	3.45	–1.23	–3.18	1.08	0.40	0.39	0.08	
	MRI-CGCM3	2.60	–1.23	–3.24	1.25	0.51	0.28	-0.03	
	NorESM1-M	2.80	–1.10	–3.17	1.32	0.45	0.29	0.01	
	NorESM1-ME		–1.10	–3.16	1.30	0.45	0.33	-0.01	
	bcc-csm1-1-m	2.86	–1.19	–3.27	1.29	0.40	0.40	0.00	
	bcc-csm1-1	2.83	–1.15	–3.21	1.27	0.45	0.28	0.05	
	inmcm4	2.08	–1.43	–3.18	1.23	0.43	0.24	-0.15	
CMIP5 mean		3.28	–1.08	–3.20	1.24	0.41	0.41	0.06	
CMIP5 standard deviation		0.74	0.29	0.05	0.09	0.10	0.33	0.14	

[END TABLE 7.SM.5 HERE]

7.SM.5 Climate metrics

7.SM.5.1 Definitions of climate metrics

Absolute Global Forcing Potential:

$$A\mathrm{GFP}_X(H) = \Delta F_X(H) \qquad \textit{Equation 7.SM.5.1}$$

Absolute Global Warming Potential

$$A\mathrm{GWP}_X(H) = \int_0^H \Delta F_X(t)dt \qquad \textit{Equation 7.SM.5.2}$$

Absolute Global Temperature-change Potential:

$$A\mathrm{GTP}^X(H) = \Delta T^X(H) = \int_0^H A\mathrm{GFP}^X(t)R_\mathrm{T}(H-t)dt \qquad \textit{Equation 7.SM.5.3}$$

Absolute Global Sea-level Rise:

$$A\mathrm{GSR}^X(H) = \Delta\mathrm{SLR}^X(H) = \int_0^H A\mathrm{GTP}^X(t)R_\mathrm{SLR}(H-t)dt$$
$$= \int_0^H \int_0^t \mathrm{AGFP}^X(t')R_\mathrm{T}(t-t')R_\mathrm{SLR}(H-t)dt'dt$$

Equation 7.SM.5.4

where R_SLR is the sea-level rise resulting from a pulse temperature increase (Sterner et al., 2014).

Increase in absolute metric ($\Delta\mathrm{AGxx}^X$) due to the carbon cycle response:

$$\Delta\mathrm{AGxx}^X = \int_0^H \int_0^t AGTP^X(t')\gamma r_F(t-t')\mathrm{AGxx}^{\mathrm{CO2}}(H-t)dt'dt \qquad \textit{Equation 7.SM.5.5}$$

where $\gamma r_F(t)$ is the CO_2 flux perturbation following a unit temperature pulse in $kgCO_2\ yr^{-1}\ K^{-1}$ using the

parameterisation of Gasser et al. (2017b), and

$$r_F = \delta(t) - \frac{\alpha_1}{\tau_1} e^{-\frac{t}{\tau_1}} - \frac{\alpha_2}{\tau_2} e^{-\frac{t}{\tau_2}} - \frac{\alpha_3}{\tau_3} e^{-\frac{t}{\tau_3}} \qquad \textit{Equation 7.SM.5.6}$$

and the parameters used in Eqs. (7.SM.4.5) and (7.SM.4.6) are given in Table 7.SM.6.

[START TABLE 7.SM.6 HERE]

Table 7.SM.6: Parameters for the carbon cycle response function (from table 1 of (Gasser et al., 2017b)).

γ ($kgCO_2\ yr^{-1}\ °C^{-1}$)	α_1	α_2	α_3	τ_1 (yr)	τ_2 (yr)	τ_3 (yr)
11.06×10^{12}	0.6368	0.3322	0.00310	2.376	30.14	490.1

[END TABLE 7.SM.6 HERE]

Metrics for step emission changes can be derived by integrating the more standard pulse emission changes up to the time horizon:

$$\mathrm{AGTP}_X^S = \int_0^H \mathrm{AGTP}_X(H-t)dt \qquad \textit{Equation 7.SM.5.7}$$

The contribution to methane emission metrics from CO_2 from methane oxidation is given by

$$\Delta\mathrm{AGxx}^X = \int_0^H Y \frac{m_{\mathrm{CO_2}}}{m_{\mathrm{CH_4}}} \frac{1}{\tau_{\mathrm{OH}}} e^{-\frac{(H-t)}{\tau_{\mathrm{OH}}}} \mathrm{AGxx}^{\mathrm{CO2}}(H-t)dt \qquad \textit{Equation 7.SM.5.8}$$

where Y is the fractional molar yield of CO_2 from CH_4 oxidation (see Section 7.6.1.3), $m_{\mathrm{CO_2}}$ and $m_{\mathrm{CH_4}}$ are the molar masses of CO_2 and CH_4, and τ_{OH} is the methane oxidation lifetime time to OH (9.7 yr; Section 6.3.1).

7.SM.5.2 Impulse response functions for GTP and Chapter 6 calculations

To generate a suite of two-layer configurations for uncertainty estimates in GTP calculations (Tables 7.SM.8–7.SM.13), information from the FaIRv1.6.2 and MAGICC7.5.1 AR6 calibration setups (Cross Chapter Box 7.1) are used. FaIRv1.6.2 uses the two-layer model in Eq. (7.SM.2.1) as its core so converting its parameters to two-layer configurations is trivial (discussed in Section 7.SM.2.2). To convert MAGICC7.5.1's configuration to two-layer configurations, the two-layer model parameters are fitted to MAGICC7.5.1's output from an abrupt $2\times CO_2$ experiment. However, such a fitting procedure produces only an approximate translation because MAGICC7.5.1 is not well-represented by a two-timescale model. After these two conversions are done an ensemble of two-layer configurations is generated which is used for uncertainty analysis in GTP calculations.

To generate the Chapter 6 two-layer configuration, the timescales and efficacy parameters are calculated as the average of FaIRv1.6.2's median and a fit to MAGICC7.5.1's median response (both in their AR6 calibrations). Response magnitudes that describe the contributions to the fast and slow response timescales are calculated such that the Chapter 6 configuration matches the best-estimate ECS of 3.0°C and TCR of 1.8°C (Table 7.13) under the best-estimate ERF due to a doubling of CO_2 of 3.93 W m^{-2}. This results in parameter values for C = 7.7 W yr m^{-2} $°C^{-1}$, C_d = 147 W yr m^{-2} $°C^{-1}$, α = –1.31 W m^{-2} $°C^{-1}$, ε = 1.03, κ =

0.88 W m^{-2} °C^{-1}. Note these parameters differ from CMIP6 two-layer model calibrations in Section 7.SM.2.1, as the set described here is derived from a constrained ensemble from two emulators.

7.SM.6 Tables of greenhouse gas lifetimes, radiative efficiencies and metrics

[START TABLE 7.SM.7 HERE]

Table 7.SM.7: Greenhouse gas lifetimes, radiative efficiencies, Global Warming Potentials (GWPs), Global Temperature Potentials (GTPs) and Cumulative Global Temperature Potentials (CGTPs). GWPs given for 20-year, 100-year and 500-year time horizons. GTPs and CGTPs given for 50-year and 100-year time horizons. Note CGTP has units of years and is applied to a change in emission rate rather than a change in emission amount. Also shown are absolute values of GWPs and GTPs (AGWPs and AGTPs), in units of picowatt years per square metre per kilogram (1 pW = 10^{-12} W). Radiative efficiencies for CH_4 and N_2O given in this table do not include chemical adjustments (values including chemical adjustments are given in Table 7.15).

Name	Formula	Lifetime (yr)	Radiative efficiency (W m^{-2} ppb^{-1})	AGWP 20 (pW m^{-2} yr kg^{-1})	GWP 20	AGWP 100 (pW m^{-2} yr kg^{-1})	GWP 100	AGWP 500 (pW m^{-2} yr kg^{-1})	GWP 500	AGTP 50 (pW m^{-2} yr kg^{-1})	GTP 50	AGTP 100 (pW m^{-2} yr kg^{-1})	GTP 100	CGTP 50 (yr)	CGTP 100 (yr)
Major Greenhouse Gases															
Carbon dioxide	CO_2		1.33×10^{-5}	0.0243	1	0.0895	1	0.314	1	0.000428	1	0.000395	1		
Methane	CH_4	11.8	0.000388	1.98	81.2	2.49	27.9	2.5	7.95	0.00473	11	0.00212	5.38	2730	3320
Nitrous oxide	N_2O	109	0.0032	6.65	273	24.5	273	40.7	130	0.124	290	0.0919	233		
Chlorofluorocarbons															
CFC-11	CCl_3F	52	0.259	181	7430	497	5560	586	1870	2.43	5670	1.25	3160		
CFC-12	CCl_2F_2	102	0.32	277	11400	998	11200	1600	5100	5.06	11800	3.66	9270		
CFC-13	$CClF_3$	640	0.278	301	12400	1450	16200	5500	17500	7.26	17000	7.4	18800		
CFC-112	CCl_2FCCl_2F	63.6	0.282	137	5620	413	4620	525	1670	2.06	4810	1.19	3020		
CFC-112a	CCl_3CClF_2	52	0.246	115	4740	317	3550	374	1190	1.55	3620	0.795	2010		
CFC-113	CCl_2FCClF_2	93	0.301	167	6860	583	6520	890	2830	2.96	6910	2.06	5210		
CFC-113a	CCl_3CF_3	55	0.241	124	5110	351	3930	422	1350	1.73	4030	0.917	2320		
CFC-114	$CClF_2CClF_2$	189	0.314	201	8260	844	9430	1930	6150	4.28	9990	3.71	9410		
CFC-114a	CCl_2FCF_3	105	0.297	183	7510	664	7420	1080	3450	3.37	7880	2.46	6240		

CFC-115	$CClF_2CF_3$	540	0.246	180	7410	859	9600	3100	9880	4.3	10100	4.33	11000		
E-R316c	trans cyc (-$CClFCF_2CF_2CClF$-)	75	0.27	117	4810	379	4230	518	1650	1.91	4450	1.2	3040		
Z-R316c	cis cyc (-$CClFCF_2CF_2CClF$-)	114	0.3	136	5590	507	5660	865	2760	2.57	6020	1.94	4910		
CFC 1112	$CClF=CClF$	0.019	0.013	0.0111	0.454	0.0113	0.126	0.0113	0.036	1.18×10^{-5}	0.028	8.96×10^{-6}	0.023	12.3	14.5
CFC 1112a	$CCl_2=CF_2$	0.006	0.007	0.00184	0.076	0.00188	0.021	0.00188	0.006	1.97×10^{-6}	0.005	1.49×10^{-6}	0.004	2.06	2.42
Hydrofluorochlorocarbons															
HCFC-21	$CHCl_2F$	1.7	0.145	14	575	14.3	160	14.3	45.6	0.0152	35.5	0.0114	29	15600	18300
HCFC-22	$CHClF_2$	11.9	0.214	139	5690	175	1960	176	560	0.336	785	0.15	379	184000	222000
HCFC-31	CH_2ClF	1.2	0.068	6.96	286	7.11	79.4	7.11	22.6	0.00752	17.6	0.00567	14.4	7750	9130
HCFC-121	$CHCl_2CCl_2F$	1.11	0.146	5.11	210	5.22	58.3	5.22	16.6	0.00552	12.9	0.00416	10.5	5690	6700
HCFC-122	$CHCl_2CClF_2$	0.9	0.159	4.94	203	5.05	56.4	5.05	16.1	0.00533	12.5	0.00403	10.2	5510	6490
HCFC-122a	$CHClFCCl_2F$	3.1	0.201	21.4	879	21.9	245	21.9	69.9	0.0236	55.3	0.0177	44.7	23800	28100
HCFC-123	$CHCl_2CF_3$	1.3	0.16	7.92	325	8.09	90.4	8.09	25.8	0.00857	20	0.00646	16.4	8830	10400
HCFC-123a	$CHClFCClF_2$	4	0.227	34.3	1410	35.3	395	35.3	113	0.0385	90	0.0285	72.3	38400	45200
HCFC-124	$CHClFCF_3$	5.9	0.207	50.3	2070	53.4	597	53.4	170	0.0612	143	0.0435	110	57700	68100
HCFC-124a	CHF_2CClF_2	17	0.25	124	5110	185	2070	186	592	0.521	1220	0.177	448	185000	232000
HCFC-132	CHClFCHClF	1.73	0.143	10.7	440	11	122	11	34.9	0.0116	27.2	0.00876	22.2	11900	14000
HCFC-132a	$CHCl_2CHF_2$	1.12	0.127	6.17	253	6.3	70.4	6.3	20.1	0.00666	15.6	0.00503	12.7	6870	8090
HCFC-132c	CH_2FCCl_2F	4.1	0.169	29.6	1220	30.6	342	30.6	97.6	0.0334	78.1	0.0247	62.7	33200	39100
HCFC-133a	CH_2ClCF_3	4.6	0.15	33.4	1370	34.7	388	34.7	111	0.0382	89.3	0.0281	71.3	37600	44400
HCFC-141	$CH_2ClCHClF$	1.14	0.072	4.08	168	4.17	46.6	4.17	13.3	0.00441	10.3	0.00333	8.43	4550	5350
HCFC-141b	CH_3CCl_2F	9.4	0.161	65.9	2710	77	860	77	246	0.115	269	0.064	162	82100	97700
HCFC-142b	CH_3CClF_2	18	0.193	134	5510	205	2300	207	658	0.611	1430	0.203	514	203000	257000
HCFC-225ca	$CHCl_2CF_2CF_3$	1.9	0.219	12	491	12.2	137	12.2	39	0.013	30.4	0.00979	24.8	13300	15700

HCFC-225cb	$CHClFCF_2CClF_2$	5.9	0.293	47.8	1960	50.8	568	50.8	162	0.0582	136	0.0414	105	54900	64800
HCFO-1233zd(E)	(E)-CF_3CH=CHCl	0.116	0.065	0.34	14	0.347	3.88	0.347	1.11	0.000364	0.851	0.000276	0.7	380	447
HCFO-1233zd(Z)	(Z)-CF_3CH=CHCl	0.036	0.025	0.0398	1.64	0.0406	0.454	0.0406	0.129	4.25×10^{-5}	0.099	3.23×10^{-5}	0.082	44.4	52.3
(e)-1-chloro-2-fluoroethene	(E/Z)-CHCl=CHF	0.005	0.001	0.00032	0.013	0.000327	0.004	0.000327	0.001	3.42×10^{-7}	0.001	2.6×10^{-6}	0.001	0.357	0.42
Hydrofluorocarbons															
HFC-23	CHF_3	228	0.191	301	12400	1310	14600	3300	10500	6.6	15400	5.95	15100		
HFC-32	CH_2F_2	5.4	0.111	65.5	2690	69	771	69	220	0.0775	181	0.0561	142	74600	88000
HFC-41	CH_3F	2.8	0.025	11.8	485	12.1	135	12.1	38.6	0.013	30.4	0.00972	24.6	13200	15500
HFC-125	CHF_2CF_3	30	0.234	164	6740	335	3740	349	1110	1.41	3300	0.512	1300		
HFC-134	CHF_2CHF_2	10	0.194	95	3900	113	1260	113	361	0.18	420	0.0944	239	120000	143000
HFC-134a	CH_2FCF_3	14	0.167	101	4140	137	1530	137	436	0.314	733	0.121	306	141000	172000
HFC-143	CH_2FCHF_2	3.6	0.128	31.7	1300	32.6	364	32.6	104	0.0353	82.6	0.0263	66.6	35400	41700
HFC-143a	CH_3CF_3	51	0.168	191	7840	520	5810	609	1940	2.53	5910	1.28	3250		
HFC-152	CH_2FCH_2F	0.471	0.045	1.89	77.6	1.93	21.5	1.93	6.14	0.00203	4.74	0.00153	3.89	2110	2480
HFC-152a	CH_3CHF_2	1.6	0.102	14.4	591	14.7	164	14.7	46.8	0.0156	36.5	0.0118	29.8	16000	18900
HFC-161	CH_3CH_2F	0.219	0.016	0.424	17.4	0.433	4.84	0.433	1.38	0.000454	1.06	0.000344	0.872	473	557
HFC-227ca	$CF_3CF_2CHF_2$	30	0.264	131	5370	267	2980	278	885	1.12	2620	0.407	1030		
HFC-227ea	CF_3CHFCF_3	36	0.273	142	5850	322	3600	345	1100	1.45	3400	0.588	1490		
HFC-236cb	$CH_2FCF_2CF_3$	13.4	0.231	91.2	3750	121	1350	121	387	0.265	620	0.106	268	125000	153000
HFC-236ea	CHF_2CHFCF_3	11.4	0.3	108	4420	134	1500	134	428	0.245	572	0.114	288	141000	170000
HFC-236fa	$CF_3CH_2CF_3$	213	0.251	181	7450	777	8690	1900	6040	3.93	9200	3.5	8870		
HFC-245ca	$CH_2FCF_2CHF_2$	6.6	0.24	65.3	2680	70.5	787	70.5	225	0.0836	196	0.0576	146	76000	89800
HFC-245cb	$CF_3CF_2CH_3$	39.9	0.251	170	6970	407	4550	445	1420	1.89	4410	0.817	2070		
HFC-245ea	$CHF_2CHFCHF_2$	3.2	0.16	22.2	912	22.8	255	22.8	72.6	0.0246	57.4	0.0183	46.5	24800	29200

HFC-245eb	CH2FCHFCF3	3.2	0.204	28.3	1160	29	325	29.1	92.6	0.0313	73.2	0.0234	59.2	31600	37200
HFC-245fa	$CHF_2CH_2CF_3$	7.9	0.245	77.1	3170	86.1	962	86.1	274	0.112	262	0.0708	180	92500	109000
HFC-263fb	$CH_3CH_2CF_3$	1.1	0.1	6.55	269	6.69	74.8	6.69	21.3	0.00707	16.5	0.00534	13.5	7300	8590
HFC-272ca	$CH_3CF_2CH_3$	9	0.08	46.4	1910	53.6	599	53.6	171	0.0771	180	0.0444	113	57300	68100
HFC-329p	$CHF_2CF_2CF_2CF_3$	32	0.313	122	5010	259	2890	272	866	1.12	2610	0.421	1070		
HFC-365mfc	$CH_3CF_2CH_2CF_3$	8.9	0.228	71.1	2920	81.7	914	81.8	261	0.117	272	0.0677	172	87400	104000
HFC-43-10mee	$CF_3CHFCHFCF_2CF_3$	17	0.357	96.3	3960	143	1600	144	458	0.403	943	0.137	347	143000	180000
HFO-1123	$CHF=CF_2$	0.004	0.002	0.000414	0.017	0.000423	0.005	0.000423	0.001	4.42×10^{-7}	0.001	3.36×10^{-7}	0.001	0.462	0.544
HFO-1132a	$CH_2=CF_2$	0.013	0.004	0.0046	0.189	0.00469	0.052	0.00469	0.015	4.91×10^{-6}	0.011	3.73×10^{-6}	0.009	5.13	6.04
HFO-1141	$CH_2=CHF$	0.007	0.002	0.00213	0.088	0.00217	0.024	0.00218	0.007	2.28×10^{-6}	0.005	1.73×10^{-6}	0.004	2.38	2.8
HFO-1225ye(Z)	(Z)-$CF_3CF=CHF$	0.027	0.025	0.0302	1.24	0.0308	0.344	0.0308	0.098	3.23×10^{-5}	0.075	2.45×10^{-5}	0.062	33.7	39.6
HFO-1225ye(E)	(E)-$CF_3CF=CHF$	0.016	0.015	0.0104	0.426	0.0106	0.118	0.0106	0.034	1.11×10^{-5}	0.026	8.41×10^{-6}	0.021	11.6	13.6
HFO-1234ze(Z)	(Z)-$CF_3CH=CHF$	0.027	0.02	0.0276	1.13	0.0282	0.315	0.0282	0.09	2.95×10^{-5}	0.069	2.24×10^{-5}	0.057	30.8	36.2
HFO-1234ze(E)	(E)-$CF_3CH=CHF$	0.052	0.045	0.12	4.94	0.123	1.37	0.123	0.391	0.000129	0.3	9.75×10^{-5}	0.247	134	158
HFO-1234yf	$CF_3CF=CH_2$	0.033	0.026	0.044	1.81	0.0449	0.501	0.0449	0.143	4.7×10^{-5}	0.11	3.57×10^{-5}	0.09	49.1	57.7
HFO-1336mzz(E)	(E)-$CF_3CH=CHCF_3$	0.334	0.132	1.57	64.3	1.6	17.9	1.6	5.09	0.00168	3.92	0.00127	3.22	1750	2050
HFO-1336mzz(Z)	(Z)-$CF_3CH=CHCF_3$	0.074	0.069	0.182	7.48	0.186	2.08	0.186	0.592	0.000195	0.455	0.000148	0.374	203	239
HFO-1243zf	$CF_3CH=CH_2$	0.025	0.015	0.0229	0.94	0.0234	0.261	0.0234	0.074	2.45×10^{-5}	0.057	1.86×10^{-5}	0.047	25.5	30
HFO-1345zfc	$CF_3CF_2CH=CH_2$	0.025	0.016	0.016	0.656	0.0163	0.182	0.0163	0.052	1.71×10^{-5}	0.04	1.29×10^{-5}	0.033	17.8	21
3,3,4,4,5,5,6,6,6-nonafluorohex-1-ene	n-$C_4F_9CH=CH_2$	0.025	0.03	0.0179	0.734	0.0182	0.204	0.0182	0.058	1.91×10^{-5}	0.045	1.45×10^{-5}	0.037	19.9	23.4
3,3,4,4,5,5,6,6,7,7,8,8,8-tridecafluorooct-1-ene	n-$C_6F_{13}CH=CH_2$	0.025	0.034	0.0142	0.584	0.0145	0.162	0.0145	0.046	1.52×10^{-5}	0.036	1.15×10^{-5}	0.029	15.9	18.7
3,3,4,4,5,5,6,6,7,7,8,8,9,9,10,10,10-heptadecafluorodec-1-ene	n-$C_8F_{17}CH=CH_2$	0.025	0.038	0.0124	0.508	0.0126	0.141	0.0126	0.04	1.32×10^{-5}	0.031	0.00001	0.025	13.8	16.2

3,3,3-trifluoro-2-(trifluoromethyl)prop-1-ene	$(CF_3)_2C=CH_2$	0.028	0.033	0.0331	1.36	0.0337	0.377	0.0337	0.107	3.53×10^{-5}	0.083	2.68×10^{-5}	0.068	36.9	43.4
1,1,2,2,3,3-hexafluorocyclopentane	cyc (-$CF_2CF_2CF_2CH_2CH_2$-)	1.6	0.2	10.5	431	10.7	120	10.7	34.2	0.0114	26.6	0.00857	21.7	11700	13800
1,1,2,2,3,3,4-heptafluorocyclopentane	cyc (-$CF_2CF_2CF_2CHFCH_2$-)	2.8	0.243	20.2	830	20.7	231	20.7	66	0.0222	52	0.0166	42.1	22500	26500
1,3,3,4,4,5,5-heptafluorocyclopentene	cyc (-$CF_2CF_2CF_2CF$=CH-)	0.61	0.215	3.95	162	4.03	45.1	4.03	12.8	0.00424	9.92	0.00321	8.14	4400	5180
(4s,5s)-1,1,2,2,3,3,4,5-octafluorocyclopentane	trans-cyc (-$CF_2CF_2CF_2CHFCHF$-)	3.2	0.259	22.5	925	23.1	258	23.1	73.6	0.0249	58.2	0.0186	47.1	25100	29600
HFO-1438ezy(E)	(E)-$(CF_3)_2CFCH=CHF$	0.334	0.079	0.721	29.6	0.736	8.22	0.736	2.34	0.000773	1.81	0.000585	1.48	804	946
HFO-1447fz	$CF_3(CF_2)_2CH=CH_2$	0.025	0.028	0.0206	0.847	0.021	0.235	0.021	0.067	2.2×10^{-5}	0.051	1.67×10^{-5}	0.042	23	27.1
1,3,3,4,4-pentafluorocyclobutene	cyc (-$CH=CFCF_2CF_2$-)	0.74	0.27	8.1	333	8.27	92.4	8.27	26.4	0.00872	20.4	0.00659	16.7	9030	10600
3,3,4,4-tetrafluorocyclobutene	cyc (-$CH=CHCF_2CF_2$-)	0.23	0.21	2.24	92.1	2.29	25.6	2.29	7.29	0.0024	5.61	0.00182	4.61	2500	2940
Chlorocarbons and Hydrochlorocarbons															
Methyl chloroform	CH_3CCl_3	5	0.065	13.8	567	14.4	161	14.4	46	0.016	37.5	0.0117	29.7	15600	18400
Carbon tetrachloride	CCl_4	32	0.166	92.7	3810	196	2200	206	658	0.849	1990	0.32	810		
Methyl chloride	CH_3Cl	0.9	0.005	0.485	19.9	0.495	5.54	0.496	1.58	0.000523	1.22	0.000395	1	541	637
Methylene chloride	CH_2Cl_2	0.493	0.029	0.978	40.2	0.998	11.2	0.998	3.18	0.00105	2.46	0.000795	2.01	1090	1280
Chloroform	$CHCl_3$	0.501	0.074	1.81	74.2	1.84	20.6	1.84	5.87	0.00194	4.53	0.00147	3.72	2010	2370
Chloroethane	CH_3CH_2Cl	0.132	0.004	0.0422	1.73	0.043	0.481	0.043	0.137	4.51×10^{-5}	0.105	3.42×10^{-5}	0.087	47	55.4
1,2-dichloroethane	CH_2ClCH_2Cl	0.225	0.009	0.114	4.68	0.116	1.3	0.116	0.371	0.000122	0.285	9.25×10^{-5}	0.234	127	150
1,1,2-trichloroethene	$CHCl=CCl_2$	0.015	0.006	0.00385	0.158	0.00393	0.044	0.00393	0.013	4.11×10^{-6}	0.01	3.12×10^{-5}	0.008	4.3	5.06
1,1,2,2-tetrachloroethene	$CCl_2=CCl_2$	0.301	0.052	0.556	22.8	0.567	6.34	0.567	1.81	0.000596	1.39	0.000451	1.14	620	730
2-chloropropane	$CH_3CHClCH_3$	0.06	0.004	0.0158	0.651	0.0162	0.181	0.0162	0.052	1.69×10^{-5}	0.04	1.28×10^{-6}	0.033	17.7	20.8
1-chlorobutane	$CH_3(CH_2)_2CH_2Cl$	0.012	0.001	0.000595	0.024	0.000607	0.007	0.000607	0.002	6.35×10^{-7}	0.001	4.82×10^{-7}	0.001	0.664	0.781
Bromocarbons, hydrobromocarbons and halons															

Methyl bromide	CH_3Br	0.8	0.004	0.213	8.74	0.217	2.43	0.217	0.692	0.000229	0.535	0.000173	0.438	237	279
Methylene bromide	CH_2Br_2	0.411	0.01	0.133	5.45	0.135	1.51	0.135	0.431	0.000142	0.333	0.000108	0.273	148	174
Halon-1201	$CHBrF_2$	4.9	0.152	32.5	1340	34	380	34	108	0.0376	88	0.0275	69.8	36800	43400
Halon-1202	CBr_2F_2	2.5	0.272	18.9	775	19.3	216	19.3	61.5	0.0207	48.4	0.0155	39.3	21000	24800
Halon-1211	$CBrClF_2$	16	0.3	120	4920	173	1930	173	552	0.458	1070	0.16	406	174000	217000
Halon-1301	$CBrF_3$	72	0.299	202	8320	644	7200	864	2750	3.23	7560	2	5060		
Halon-2301	CH_2BrCF_3	3.2	0.135	15.5	635	15.9	177	15.9	50.6	0.0171	40	0.0128	32.4	17200	20300
Halon-2311	$CHBrClCF_3$	1	0.133	3.94	162	4.03	45	4.03	12.8	0.00425	9.95	0.00321	8.14	4400	5170
Halon-2401	$CHBrFCF_3$	2.9	0.189	17.6	723	18	201	18	57.5	0.0194	45.3	0.0145	36.7	19600	23100
Halon-2402	$CBrF_2CBrF_2$	28	0.312	99	4070	194	2170	201	639	0.791	1850	0.277	702		
Tribromomethane	$CHBr_3$	0.156	0.006	0.0219	0.901	0.0224	0.25	0.0224	0.071	2.35×10^{-5}	0.055	0.0000178	0.045	24.5	28.8
Halon-1011	CH_2BrCl	0.452	0.02	0.415	17.1	0.424	4.74	0.424	1.35	0.000446	1.04	0.000337	0.855	463	545
Bromoethane	CH_3CH_2Br	0.137	0.006	0.0427	1.75	0.0436	0.487	0.0436	0.139	4.57×10^{-5}	0.107	3.46×10^{-5}	0.088	47.6	56
1,2-dibromoethane	CH_2BrCH_2Br	0.244	0.012	0.0894	3.67	0.0913	1.02	0.0913	0.291	9.58×10^{-5}	0.224	7.26×10^{-5}	0.184	99.7	117
1-bromopropane	$CH_3CH_2CH_2Br$	0.041	0.002	0.00457	0.188	0.00466	0.052	0.00466	0.015	4.88×10^{-6}	0.011	3.71×10^{-6}	0.009	5.1	6
2-bromopropane	$CH_3CHBrCH_3$	0.055	0.004	0.011	0.453	0.0112	0.126	0.0112	0.036	1.18×10^{-5}	0.028	8.93×10^{-6}	0.023	12.3	14.5
Fully fluorinated species															
Nitrogen trifluoride	NF_3	569	0.204	326	13400	1560	17400	5720	18200	7.81	18200	7.89	20000		
Pentadecafluorotriethylamine	$N(C_2F_5)_3$	1000	0.61	188	7700	923	10300	3860	12300	4.61	10800	4.81	12200		
Perfluorotripropylamine	$N(CF_2CF_2CF_3)_3$	1000	0.75	164	6750	808	9030	3380	10800	4.03	9430	4.21	10700		
Heptacosafluorotributylamine	$N(CF_2CF_2CF_2CF_3)_3$	1000	0.907	154	6340	759	8490	3170	10100	3.79	8860	3.96	10000		
Perfluorotripentylamine	$N(CF_2CF_2CF_2CF_2CF_3)_3$	1000	0.95	132	5420	650	7260	2720	8650	3.24	7580	3.39	8580		
Heptafluoroisobutyronitrile	$(CF_3)_2CFCN$	34.5	0.248	111	4580	246	2750	262	835	1.09	2560	0.431	1090		
Sulfur hexafluoride	SF_6	3200	0.567	445	18300	2250	25200	10700	34100	11.2	26200	12.1	30600		

Trifluromethylsulfur pentafluoride	SF_5CF_3	800	0.585	339	13900	1660	18500	6610	21100	8.27	19300	8.54	21600		
Sulfuryl fluoride	SO_2F_2	36	0.211	183	7510	414	4630	444	1410	1.87	4360	0.756	1920		
PFC-14	CF_4	50000	0.099	129	5300	660	7380	3320	10600	3.28	7660	3.57	9050		
PFC-116	C_2F_6	10000	0.261	218	8940	1110	12400	5500	17500	5.51	12900	5.99	15200		
PFC-218	C_3F_8	2600	0.27	165	6770	831	9290	3890	12400	4.13	9660	4.44	11200		
Hexafluorocyclobutene	cyc (-CF=CFCF$_2$CF$_2$-)	1.02	0.3	11	453	11.3	126	11.3	35.9	0.0119	27.8	0.00898	22.8	12300	14500
PFC-C-318	cyc (-CF$_2$CF$_2$CF$_2$CF$_2$-)	3200	0.314	180	7400	912	10200	4330	13800	4.53	10600	4.88	12400		
PFC-31-10	n-C_4F_{10}	2600	0.369	178	7300	897	10000	4200	13400	4.46	10400	4.79	12100		
Octafluorocyclopentene	cyc (-CF=CFCF$_2$CF$_2$CF$_2$-)	1.1	0.246	6.84	281	6.99	78.1	6.99	22.3	0.00739	17.3	0.00557	14.1	7620	8970
PFC-41-12	n-C_5F_{12}	4100	0.408	163	6680	825	9220	3970	12700	4.1	9580	4.43	11200		
PFC-51-14	n-C_6F_{14}	3100	0.449	153	6260	771	8620	3660	11600	3.83	8960	4.12	10500		
PFC-61-16	n-C_7F_{16}	3000	0.503	149	6120	752	8410	3560	11300	3.74	8740	4.02	10200		
PFC-71-18	n-C_8F_{18}	3000	0.558	146	6010	739	8260	3500	11100	3.67	8590	3.95	10000		
PFC-91-18	$C_{10}F_{18}$	2000	0.537	133	5480	669	7480	3070	9780	3.33	7790	3.56	9010		
1,1,2,2,3,3,4,4,4a,5,5,6,6,7,7,8,8, 8a-octadecafluoronaphthalene	Z-$C_{10}F_{18}$	2000	0.56	139	5710	698	7800	3200	10200	3.47	8120	3.71	9400		
1,1,2,2,3,3,4,4,4a,5,5,6,6,7,7,8,8, 8a-octadecafluoronaphthalene	E-$C_{10}F_{18}$	2000	0.512	127	5220	637	7120	2920	9310	3.17	7420	3.39	8580		
PFC-1114	$CF_2=CF_2$	0.003	0.002	0.000347	0.014	0.000354	0.004	0.000354	0.001	3.71×10^{-7}	0.001	2.81×10^{-7}	0.001	0.387	0.456
PFC-1216	$CF_3CF=CF_2$	0.015	0.013	0.00788	0.324	0.00804	0.09	0.00804	0.026	8.42×10^{-6}	0.02	6.39×10^{-6}	0.016	8.8	10.3
1,1,2,3,4,4-hexafluorobuta-1,3-diene	$CF_2=CFCF=CF_2$	0.003	0.003	0.000347	0.014	0.000354	0.004	0.000354	0.001	3.71×10^{-7}	0.001	2.82×10^{-7}	0.001	0.388	0.456
Octafluoro-1-butene	$CF_3CF_2CF=CF_2$	0.016	0.019	0.00891	0.366	0.00909	0.102	0.00909	0.029	9.52×10^{-6}	0.022	7.22×10^{-5}	0.018	9.94	11.7
Octafluoro-2-buene	$CF_3CF=CFCF_3$	0.085	0.07	0.173	7.1	0.176	1.97	0.176	0.562	0.000185	0.432	0.00014	0.355	193	227
Halogenated alcohols, ethers, furans, aldehydes and ketones															

HFE-125	CHF_2OCF_3	135	0.417	328	13500	1280	14300	2410	7680	6.5	15200	5.17	13100		
HFE-134	CHF_2OCHF_2	26.9	0.449	310	12700	593	6630	610	1940	2.37	5530	0.814	2060		
HFE-143a	CH_3OCF_3	4.9	0.189	52.8	2170	55.1	616	55.1	176	0.0611	143	0.0447	113	59700	70400
HFE-227ea	$CF_3CHFOCF_3$	54.8	0.459	238	9800	673	7520	808	2570	3.3	7720	1.75	4440		
HCFE-235ca2	CHF_2OCF_2CHFCl	4.42	0.409	56.4	2320	58.5	654	58.5	186	0.0642	150	0.0473	120	63400	74800
HCFE-235da2	$CHF_2OCHClCF_3$	3.5	0.426	46.9	1930	48.2	539	48.2	154	0.0522	122	0.0388	98.4	52400	61700
HCFE-236ea2	$CHF_2OCHFCF_3$	14.1	0.464	171	7020	232	2590	233	741	0.537	1260	0.206	521	239000	292000
HFE-236fa	$CF_3CH_2OCF_3$	7.5	0.371	89.4	3670	98.7	1100	98.8	315	0.125	291	0.0811	205	106000	126000
HFE-245cb2	$CF_3CF_2OCH_3$	5	0.336	64	2630	66.9	747	66.9	213	0.0743	174	0.0542	137	72400	85400
HFE-245fa1	$CHF_2CH_2OCF_3$	6.7	0.314	77.2	3170	83.6	934	83.6	266	0.0998	233	0.0683	173	90100	106000
HFE-245fa2	$CHF_2OCH_2CF_3$	5.5	0.36	74.5	3060	78.6	878	78.6	251	0.0886	207	0.0639	162	85000	100000
2,2,3,3,3-pentafluoropropan-1-ol	$CF_3CF_2CH_2OH$	0.471	0.164	3.01	123	3.07	34.3	3.07	9.78	0.00323	7.54	0.00244	6.19	3350	3940
HFE-254cb1	$CH_3OCF_2CHF_2$	2.5	0.26	28.7	1180	29.3	328	29.3	93.5	0.0314	73.4	0.0235	59.6	31900	37600
HFE-263mf	$CF_3CH_2OCH_3$	0.077	0.046	0.181	7.43	0.184	2.06	0.185	0.588	0.000193	0.452	0.000147	0.371	202	237
HFE-263m1	$CF_3OCH_2CH_3$	0.397	0.126	2.56	105	2.61	29.2	2.61	8.32	0.00274	6.42	0.00208	5.27	2850	3360
3,3,3-trifluoropropan-1-ol	$CF_3CH_2CH_2OH$	0.041	0.026	0.0544	2.23	0.0555	0.62	0.0555	0.177	5.81×10^{-5}	0.136	4.41×10^{-5}	0.112	60.7	71.4
HFE-329mcc2	$CHF_2CF_2OCF_2CF_3$	25	0.545	184	7550	337	3770	345	1100	1.29	3020	0.432	1090		
HFE-338mmz1	$(CF_3)_2CHOCHF_2$	22.3	0.452	158	6500	272	3040	276	880	0.967	2260	0.314	797		
HFE-338mcf2	$CF_3CH_2OCF_2CF_3$	7.5	0.454	84.2	3460	93	1040	93.1	297	0.117	274	0.0764	194	100000	118000
HFE-347mmz1	$(CF_3)_2CHOCH_2F$	1.9	0.308	17.1	702	17.5	195	17.5	55.7	0.0186	43.5	0.014	35.4	19000	22400
HFE-347mcc3	$CH_3OCF_2CF_2CF_3$	5.1	0.339	49.2	2020	51.5	576	51.6	164	0.0574	134	0.0418	106	55800	65800
HFE-347mcf2	$CHF_2CH_2OCF_2CF_3$	6.7	0.431	79.6	3270	86.2	963	86.2	275	0.103	241	0.0705	179	92900	110000
HFE-347pcf2	$CHF_2CF_2OCH_2CF_3$	6.1	0.482	82.1	3370	87.6	980	87.7	279	0.101	237	0.0715	181	94700	112000
HFE-347mmy1	$(CF_3)_2CFOCH_3$	3.7	0.318	34.1	1400	35.1	392	35.1	112	0.0381	89	0.0283	71.8	38100	44900

HFE-356mec3	$CH_3OCF_2CHFCF_3$	2.5	0.288	23.1	949	23.6	264	23.6	75.3	0.0253	59.2	0.019	48	25700	30300
HFE-356mff2	$CF_3CH_2OCH_2CF_3$	0.351	0.19	2.14	88	2.19	24.4	2.19	6.97	0.0023	5.37	0.00174	4.41	2390	2810
HFE-356pcf2	$CHF_2CH_2OCF_2CHF_2$	6	0.378	69.8	2870	74.4	831	74.4	237	0.0856	200	0.0606	154	80400	94800
HFE-356pcf3	$CHF_2OCH_2CF_2CHF_2$	3.5	0.378	42.1	1730	43.3	484	43.3	138	0.0469	110	0.0349	88.4	47000	55400
HFE-356pcc3	$CH_3OCF_2CF_2CHF_2$	2.5	0.303	24.2	995	24.8	277	24.8	79	0.0266	62.1	0.0199	50.4	27000	31800
HFE-356mmz1	$(CF_3)_2CHOCH_3$	0.178	0.125	0.713	29.3	0.728	8.13	0.728	2.32	0.000763	1.78	0.000579	1.47	795	936
HFE-365mcf3	$CF_3CF_2CH_2OCH_3$	0.069	0.058	0.141	5.77	0.143	1.6	0.143	0.457	0.00015	0.351	0.000114	0.289	157	184
HFE-374pc2	$CHF_2CF_2OCH_2CH_3$	0.208	0.132	1.1	45	1.12	12.5	1.12	3.56	0.00117	2.74	0.000889	2.25	1220	1440
4,4,4-trifluorobutan-1-ol	$CF_3(CH_2)_2CH_2OH$	0.015	0.006	0.00433	0.178	0.00442	0.049	0.00442	0.014	4.63×10^{-5}	0.011	3.51×10^{-5}	0.009	4.84	5.69
2,2,3,3,4,4,5,5-octafluorocyclopentan-1-ol	cyc (-$(CF_2)_4CH(OH)$-)	0.301	0.156	1.2	49.1	1.22	13.6	1.22	3.89	0.00128	3	0.000971	2.46	1330	1570
HFE-43-10pccc124	$CHF_2OCF_2OCF_2CF_2OCHF_2$	14.1	1.03	212	8720	288	3220	289	920	0.667	1560	0.255	647	297000	363000
HFE-449s1	$C_4F_9OCH_3$	4.8	0.36	39.5	1620	41.2	460	41.2	131	0.0455	106	0.0334	84.6	44600	52600
n-HFE-7100	$CF_3CF_2CF_2CF_2OCH_3$	4.8	0.425	46.7	1920	48.6	544	48.7	155	0.0538	126	0.0394	99.9	52700	62200
i-HFE-7100	$(CF_3)_2CFCF_2OCH_3$	4.8	0.341	37.5	1540	39.1	437	39.1	124	0.0432	101	0.0317	80.2	42300	49900
HFE-569sf2	$C_4F_9OC_2H_5$	0.8	0.301	5.32	219	5.43	60.7	5.43	17.3	0.00573	13.4	0.00433	11	5930	6980
i-HFE-7200	$(CF_3)_2CFCF_2OCH_2CH_3$	0.63	0.216	3.01	124	3.07	34.3	3.07	9.78	0.00323	7.56	0.00245	6.2	3350	3950
HFE-7300	$(CF_3)_2CFCFOC_2H_5CF_2CF_2CF_3$	5.24	0.48	34.5	1420	36.2	405	36.2	115	0.0405	94.7	0.0294	74.6	39200	46200
HFE-7500	n-$C_3F_7CFOC_2H_5CF(CF_3)_2$	0.3	0.27	1.14	47	1.17	13	1.17	3.72	0.00123	2.86	0.000928	2.35	1270	1500
HFE-236ca12	$CHF_2OCF_2OCHF_2$	26.5	0.648	285	11700	542	6060	557	1770	2.15	5020	0.733	1860		
HFE-338pcc13	$CHF_2OCF_2CF_2OCHF_2$	13.4	0.87	223	9180	297	3320	297	948	0.649	1520	0.259	657	307000	374000
1,1,1,3,3,3-hexafluoropropan-2-ol	$(CF_3)_2CHOH$	1.9	0.274	18.1	742	18.5	206	18.5	58.8	0.0197	46	0.0148	37.4	20100	23700
HG-02	$CHF_2(OCF_2CF_2)_2OCHF_2$	26.9	1.15	268	11000	513	5730	528	1680	2.05	4780	0.704	1780		
HG-03	$CHF_2(OCF_2CF_2)_3OCHF_2$	26.9	1.43	250	10300	479	5350	492	1570	1.91	4470	0.657	1660		

Fluroxene	$CF_3CH_2OCH=CH_2$	0.01	0.011	0.00505	0.207	0.00515	0.058	0.00515	0.016	5.39×10^{-5}	0.013	4.09×10^{-6}	0.01	5.63	6.63
2-ethoxy-3,3,4,4,5-pentafluorotetrahydro-2,5-bis[1,2,2,2-tetrafluoro-1-(trifluoromethyl)ethyl]-furan	$C_{12}H_5F_{19}O_2$	0.81	0.489	4.27	175	4.36	48.7	4.36	13.9	0.0046	10.7	0.00347	8.8	4760	5600
Difluoro(methoxy)methane	CH_3OCHF_2	1.1	0.153	11.9	491	12.2	136	12.2	38.9	0.0129	30.1	0.00973	24.7	13300	15700
HG'-01	$CH_3OCF_2CF_2OCH_3$	1.7	0.289	17.7	727	18.1	202	18.1	57.7	0.0192	45	0.0145	36.7	19700	23200
HG'-02	$CH_3O(CF_2CF_2O)_2CH_3$	1.7	0.562	20	823	20.5	229	20.5	65.3	0.0218	50.9	0.0164	41.5	22300	26300
HG'-03	$CH_3O(CF_2CF_2O)_3CH_3$	1.7	0.762	19.2	789	19.6	219	19.6	62.5	0.0209	48.8	0.0157	39.8	21400	25200
HFE-329me3	$CF_3CFHCF_2OCF_3$	33.6	0.489	180	7410	393	4390	416	1330	1.73	4040	0.671	1700		
3,3,4,4,5,5,6,6,7,7,7-undecafluoroheptan-1-ol	$CF_3(CF_2)_4CH_2CH_2OH$	0.047	0.054	0.0468	1.92	0.0477	0.533	0.0477	0.152	5×10^{-5}	0.117	3.79×10^{-5}	0.096	52.2	61.4
3,3,4,4,5,5,6,6,7,7,8,8,9,9,9-pentadecafluorononan-1-ol	$CF_3(CF_2)_6CH_2CH_2OH$	0.047	0.06	0.0394	1.62	0.0401	0.449	0.0402	0.128	4.21×10^{-5}	0.098	3.19×10^{-5}	0.081	43.9	51.7
3,3,4,4,5,5,6,6,7,7,8,8,9,9,10,10,11,11,11-nonadecafluoroundecan-1-ol	$CF_3(CF_2)_8CH_2CH_2OH$	0.047	0.045	0.024	0.985	0.0245	0.273	0.0245	0.078	2.56×10^{-5}	0.06	1.94×10^{-5}	0.049	26.8	31.5
2-chloro-1,1,2-trifluoro-1-methoxyethane	CH_3OCF_2CHClF	1.43	0.211	11.9	488	12.1	136	12.1	38.7	0.0129	30.1	0.0097	24.6	13200	15600
PFPMIE	$CF_3OCFCF_3CF_2OCF_2OCF_3$	800	0.64	189	7750	920	10300	3680	11700	4.59	10700	4.75	12000		
HFE-216	$CF_3OCF=CF_2$	0.004	0.006	0.000909	0.037	0.000927	0.01	0.000928	0.003	9.71×10^{-7}	0.002	7.37×10^{-7}	0.002	1.01	1.19
Perfluoroethyl formate	CF_3CF_2OCHO	3.6	0.408	51.9	2130	53.4	597	53.4	170	0.0579	135	0.0431	109	58000	68400
2,2,2-trifluoroethyl formate	CF_3CH_2OCHO	0.548	0.192	4.8	197	4.9	54.8	4.9	15.6	0.00516	12.1	0.0039	9.89	5350	6300
Formic acid;1,1,1,3,3,3-hexafluoropropan-2-ol	$(CF_3)_2CHOCHO$	3.1	0.255	23.5	964	24.1	269	24.1	76.7	0.0259	60.6	0.0194	49	26100	30800
Ethenyl 2,2,2-trifluoroacetate	$CF_3COOCH=CH_2$	0.004	0.004	0.000705	0.029	0.000719	0.008	0.000719	0.002	7.52×10^{-7}	0.002	5.71×10^{-7}	0.001	0.786	0.925
Ethyl 2,2,2-trifluoroacetate	$CF_3COOCH_2CH_3$	0.06	0.056	0.139	5.7	0.142	1.58	0.142	0.451	0.000148	0.347	0.000112	0.285	155	182
Prop-2-enyl 2,2,2-trifluoroacetate	$CF_3COOCH_2CH=CH_2$	0.003	0.005	0.000636	0.026	0.000648	0.007	0.000649	0.002	6.79×10^{-7}	0.002	5.15×10^{-7}	0.001	0.71	0.835

Methyl 2,2,2-trifluoroacetate	CF_3COOCH_3	1	0.158	7.21	296	7.36	82.3	7.36	23.5	0.00778	18.2	0.00587	14.9	8030	9460
2,2,3,3,4,4,4-heptafluorobutan-1-ol	$CF_3CF_2CF_2CH_2OH$	0.55	0.199	3.2	131	3.26	36.5	3.26	10.4	0.00343	8.03	0.0026	6.58	3560	4190
1,1,2-trifluoro-2-(trifluoromethoxy)ethane	$CHF_2CHFOCF_3$	9	0.353	97.6	4010	113	1260	113	359	0.162	379	0.0933	236	120000	143000
1-ethoxy-1,1,2,3,3,3-hexafluoropropane	$CF_3CHFCF_2OCH_2CH_3$	0.403	0.193	2.32	95.2	2.37	26.4	2.37	7.54	0.00249	5.81	0.00188	4.77	2580	3040
1,1,1,2,2,3,3-heptafluoro-3-(1,2,2,2-tetrafluoroethoxy)propane	$CF_3CF_2CF_2OCHFCF_3$	59.4	0.591	202	8320	593	6630	733	2340	2.94	6860	1.63	4140		
2,2,3,3-tetrafluoropropan-1-ol	$CHF_2CF_2CH_2OH$	0.255	0.112	1.27	52	1.29	14.4	1.29	4.12	0.00136	3.17	0.00103	2.6	1410	1660
2,2,3,4,4,4-hexafluorobutan-1-ol	$CF_3CHFCF_2CH_2OH$	0.367	0.227	2.67	110	2.73	30.5	2.73	8.69	0.00287	6.7	0.00217	5.5	2980	3510
1,1,2,2-tetrafluoro-3-methoxypropane	$CHF_2CF_2CH_2OCH_3$	0.071	0.052	0.147	6.03	0.15	1.68	0.15	0.478	0.000157	0.367	0.000119	0.302	164	193
1,1,1,2,2,4,5,5,5-nonafluoro-4-(trifluoromethyl)pentan-3-one	$CF_3CF_2COCF(CF_3)_2$	0.019	0.028	0.01	0.411	0.0102	0.114	0.0102	0.033	1.07×10^{-5}	0.025	8.12×10^{-5}	0.021	11.2	13.1
3,3,3-trifluoropropanal	CF_3CH_2CHO	0.008	0.005	0.00221	0.091	0.00225	0.025	0.00225	0.007	2.36×10^{-5}	0.006	1.79×10^{-5}	0.005	2.46	2.9
2-fluoroethanol	CH_2FCH_2OH	0.044	0.012	0.0465	1.91	0.0474	0.53	0.0474	0.151	4.97×10^{-5}	0.116	3.77×10^{-5}	0.095	51.9	61
2,2-difluoroethanol	CHF_2CH_2OH	0.167	0.046	0.542	22.3	0.553	6.18	0.553	1.76	0.00058	1.36	0.00044	1.11	605	711
2,2,2-trifluoroethanol	CF_3CH_2OH	0.458	0.117	3.13	129	3.2	35.7	3.2	10.2	0.00336	7.86	0.00254	6.44	3490	4110
HG-04	$CHF_2O(CF_2CF_2O)_4CHF_2$	26.9	1.46	204	8400	392	4380	403	1280	1.56	3660	0.538	1360		
Methyl-perfluoroheptene-ethers	$CH_3OC_7F_{13}$	0.304	0.27	1.32	54.4	1.35	15.1	1.35	4.3	0.00142	3.31	0.00107	2.72	1480	1740
1,1,1-trifluoropropan-2-one	CF_3COCH_3	0.014	0.011	0.00788	0.324	0.00804	0.09	0.00804	0.026	8.42×10^{-5}	0.02	6.39×10^{-5}	0.016	8.79	10.3
1,1,1-trifluorobutan-2-one	$CF_3COCH_2CH_3$	0.018	0.01	0.00834	0.343	0.00851	0.095	0.00851	0.027	8.91×10^{-5}	0.021	6.76×10^{-5}	0.017	9.31	11
1-chloro-2-ethenoxyethane	$ClCH_2CH_2OCH=CH_2$	0	0.001	1.65×10^{-5}	0.001	1.68×10^{-5}	0	1.68×10^{-5}	0	1.76×10^{-8}	0	1.33×10^{-8}	0	0.018	0.022
2-methylpentan-3-one	$CH_3CH_2COCH(CH_3)_2$	0.015	0.02	0.0175	0.719	0.0179	0.2	0.0179	0.057	1.87×10^{-5}	0.044	1.42×10^{-5}	0.036	19.5	23
Ethyl methyl ether	$CH_3CH_2OCH_3$	0.005	0.002	0.000856	0.035	0.000873	0.01	0.000873	0.003	9.14×10^{-7}	0.002	6.94×10^{-7}	0.002	0.955	1.12
Octafluorooxolane	$c\text{-}C_4F_8O$	3000	0.463	246	10100	1240	13900	5890	18800	6.18	14500	6.65	16900		

Crotonaldehyde	$CH_3CH=CHCHO$	0.001	0	0	0	0	0	0	0	0	0	0	0	0	0
Methyl vinyl ketone	$CH_3COCH=CH_2$	0.001	0	2.48×10^{-5}	0.001	2.53×10^{-5}	0	2.53×10^{-5}	0	2.64×10^{-8}	0	2.01×10^{-8}	0	0.028	0.033
Allyl ether	$(CH_2=CHCH_2)_2O$	0	0.001	1.19×10^{-5}	0	1.22×10^{-5}	0	1.22×10^{-5}	0	1.27×10^{-8}	0	9.65×10^{-9}	0	0.013	0.016
Allyl ethyl ether	$CH_3CH_2OCH_2CH=CH_2$	0.001	0.001	3.39×10^{-5}	0.001	3.46×10^{-5}	0	3.46×10^{-5}	0	3.62×10^{-8}	0	2.75×10^{-8}	0	0.038	0.045
(z)-hex-2-en-1-ol	$CH_3CH_2CH_2CH=CHCH_2OH$	0	0.038	0.000223	0.009	0.000228	0.003	0.000228	0.001	2.38×10^{-7}	0.001	1.81×10^{-7}	0	0.249	0.293
(e)-hex-2-en-1-ol	$CH_3CH_2CH_2CH=CHCH_2OH$	0	0.036	0.000208	0.009	0.000212	0.002	0.000212	0.001	2.22×10^{-7}	0.001	1.68×10^{-7}	0	0.232	0.273
Miscellaneous compounds															
Allyl cyanide	$CH_2=CHCH_2CN$	0.002	0	4.08×10^{-5}	0.002	4.16×10^{-5}	0	4.16×10^{-5}	0	4.35×10^{-8}	0	3.3×10^{-8}	0	0.045	0.054
Hexamethyldisiloxane	$C_6H_{18}OSi_2$	0.025	0.047	0.0418	1.72	0.0426	0.476	0.0426	0.136	4.46×10^{-5}	0.104	3.39×10^{-5}	0.086	46.6	54.8
Octamethyltrisiloxane	$C_8H_{24}O_2Si_3$	0.019	0.06	0.0285	1.17	0.029	0.325	0.029	0.093	3.04×10^{-5}	0.071	2.31×10^{-5}	0.058	31.8	37.4
Decamethyltetrasiloxane	$C_{10}H_{30}O_3Si_4$	0.014	0.06	0.0155	0.635	0.0158	0.176	0.0158	0.05	1.65×10^{-5}	0.039	1.25×10^{-5}	0.032	17.3	20.3
Dodecamethylpentasiloxane	$C_{12}H_{36}O_4Si_5$	0.011	0.064	0.0107	0.439	0.0109	0.122	0.0109	0.035	1.14×10^{-5}	0.027	8.67×10^{-6}	0.022	11.9	14
Hexamethylcyclotrisiloxane	$C_6H_{18}O_3Si_3$	0.038	0.1	0.101	4.14	0.103	1.15	0.103	0.328	0.000108	0.252	8.18×10^{-5}	0.207	113	132
Octamethylcyclotetrasiloxane	$C_8H_{24}O_4Si_4$	0.027	0.12	0.0648	2.66	0.0661	0.739	0.0661	0.211	6.92×10^{-5}	0.162	5.25×10^{-5}	0.133	72.3	85.1
Decamethylcyclopentasiloxane	$C_{10}H_{30}O_5Si_5$	0.016	0.098	0.0253	1.04	0.0258	0.289	0.0259	0.082	2.71×10^{-5}	0.063	2.05×10^{-5}	0.052	28.3	33.3
Dodecamethylcyclohexasiloxane	$C_{12}H_{36}O_6Si_6$	0.011	0.086	0.0124	0.51	0.0127	0.142	0.0127	0.04	1.33×10^{-5}	0.031	1.01×10^{-5}	0.026	13.9	16.3
Ethane	C_2H_6	0.159	0.001	0.0383	1.57	0.0391	0.437	0.0391	0.125	4.1×10^{-5}	0.096	3.11×10^{-5}	0.079	42.7	50.3
Propane	C_3H_8	0.036	0	0.00175	0.072	0.00178	0.02	0.00178	0.006	1.87×10^{-6}	0.004	1.42×10^{-6}	0.004	1.95	2.29
Butane	$n\text{-}C_4H_{10}$	0.019	0	0.000542	0.022	0.000553	0.006	0.000553	0.002	5.79×10^{-7}	0.001	4.4×10^{-7}	0.001	0.605	0.712

[END TABLE 7.SM.7 HERE]

[START TABLE 7.SM.8 HERE]

Table 7.SM.8: Estimated uncertainty in the GWP and GTP for CH_4 showing the total uncertainty as a percentage of the best estimate (expressed as 5-95% confidence interval), and the uncertainty by component of the total emission metric calculation (radiative efficiency, chemistry feedbacks, atmospheric lifetime, CO_2 (combined uncertainty in radiative efficiency and CO_2 impulse response), carbon cycle response, fate of oxidized fossil methane, and impulse-response function. Uncertainties in individual terms are taken from Section 7.6, except for the CO_2 impulse response which comes from (Joos et al., 2013). The impulse-response uncertainties are calculated by taking 1.645×standard deviation of the GTPs generated from 600 ensemble members of the impulse response derived from FaIRv1.6.2 and MAGICC7.5.1 (Section 7.SM.4.2)

Metric	Percentage uncertainty in the metric best estimate due to							Total uncertainty (%)
	Radiative efficiency (%)	Chemical response (%)	Lifetime (%)	CO_2 (%)	Carbon cycle (%)	Fossil fuel oxidation (%)	Impulse Response function (%)	
GWP20	20	14	9	18	3	2	0	32
GWP100	20	14	14	26	5	7	0	40
GWP500	20	14	14	29	5	26	0	48
GTP50	20	14	37	22	17	22	31	64
GTP100	20	14	18	28	8	60	38	83

[END TABLE 7.SM.8 HERE]

[START TABLE 7.SM.9 HERE]

Table 7.SM.9: As Table 7.SM.8, for N_2O

Metric	Percentage uncertainty in the metric best estimate due to						Total uncertainty (%)
	Radiative efficiency (%)	Chemical response (%)	Lifetime (%)	CO_2 (%)	Carbon cycle (%)	Impulse Response function (%)	
GWP20	16	36	1	18	2	0	43
GWP100	16	36	3	26	5	0	47
GWP500	16	36	8	29	5	0	49
GTP50	16	36	3	25	6	1	46
GTP100	16	36	7	29	6	2	49

[END TABLE 7.SM.9 HERE]

[START TABLE 7.SM.10 HERE]

Table 7.SM.10: As Table 7.SM.8, for CFC-11

Metric	Percentage uncertainty in the metric best estimate due to					Total uncertainty (%)
	Radiative efficiency (%)	Lifetime (%)	CO_2 (%)	Carbon cycle (%)	Impulse Response function (%)	
GWP20	22	3	18	2	0	29
GWP100	22	12	26	5	0	37
GWP500	22	19	29	5	0	42
GTP50	22	14	24	6	4	37
GTP100	22	28	28	7	7	47

[ENDTABLE 7.SM.10 HERE]

[START TABLE 7.SM.11 HERE]

Table 7.SM.11: As Table 7.SM.8, for PFC-14 (CF_4)

Metric	Percentage uncertainty in the metric best estimate due to					Total uncertainty (%)
	Radiative efficiency (%)	Lifetime (%)	CO_2 (%)	Carbon cycle (%)	Impulse Response function (%)	
GWP20	19	0	18	2	0	26
GWP100	19	0	26	4	0	33
GWP500	19	0	29	5	0	35
GTP50	19	0	25	5	2	32
GTP100	19	0	29	5	1	35

[END TABLE 7.SM.11 HERE]

[START TABLE 7.SM.12 HERE]

Table 7.SM.12: As Table 7.SM.8, for HFC-134a

Metric	Percentage uncertainty in the metric best estimate due to					Total uncertainty (%)
	Radiative efficiency (%)	Lifetime (%)	CO_2 (%)	Carbon cycle (%)	Impulse Response function (%)	
GWP20	19	10	18	3	0	28
GWP100	19	19	26	5	0	38

GWP500	19	19	29	5	0	40
GTP50	19	47	22	14	25	62
GTP100	19	30	28	9	37	59

[END TABLE 7.SM.12 HERE]

[START TABLE 7.SM.13 HERE]

Table 7.SM.13: As Table 7.SM.8, for HFC-32

Metric	Percentage uncertainty in the metric best estimate due to					Total uncertainty (%)
	Radiative efficiency (%)	Lifetime (%)	CO_2 (%)	Carbon cycle (%)	Impulse Response function (%)	
GWP20	19	17	18	3	0	31
GWP100	19	19	26	5	0	38
GWP500	19	19	29	5	0	40
GTP50	19	22	19	26	48	65
GTP100	19	19	29	7	39	56

[END TABLE 7.SM.13 HERE]

7.SM.7 Data Table

[START TABLE 7.SM.14 HERE]

Table 7.SM.14: Input Data Table. Input datasets and code used to create chapter figures.

Figure number / Table number / Chapter section (for calculations)	Dataset / Code name	Type	Filename / Specificities	License type	Dataset / Code citation	Dataset / Code URL	Related publications
Box 7.2, Figure 1		Code	notebooks/350_chapter7_box7.2_fig1.ipynb	MIT	(Smith et al., 2021) [original author Matthew Palmer]	https://github.com/chrisroadmap/ar6	
Box 7.2, Figure 1		Data	data_input/fig7.1_box7.2/			https://github.com/chrisroadmap/ar6	
Figure 7.3		Code	notebooks/300_chapter7_fig7.3.ipynb	MIT	(Smith et al., 2021) [original author Matthew Palmer]	https://github.com/chrisroadmap/ar6	
Figure 7.3		Data	data_input/Loeb_et_al_2020			https://github.com/chrisroadmap/ar6	(Loeb et al., 2020)
Figure 7.4		Code	notebooks/270_chapter7_fig7.4.ipynb	MIT	(Smith et al., 2021)	https://github.com/chrisroadmap/ar6	

Figure 7.4		Data	data_input/Marshall_et_al_2020_GRL data_input/Smith_et_al_ACP_2020 data_input/Smith_et_al_GRL_2018 data_input/Hodnebrog_et_al_2020_npj			https://github.com/chrisroadmap/ar6	(Smith et al., 2018b, 2020; Hodnebrog et al., 2020; Marshall et al., 2020)
Figure 7.5		Code	notebooks/060_chapter7_fig7.5_SPM_fig15.ipynb	MIT	(Smith et al., 2021)	https://github.com/chrisroadmap/ar6	
Figure 7.5		Data	data_input/Smith_et_al_ACP_2020			https://github.com/chrisroadmap/ar6	(Zelinka et al., 2014; Smith et al., 2020)
Figure 7.6		Code	notebooks/100_chapter7_fig7.6.ipynb	MIT	(Smith et al., 2021)	https://github.com/chrisroadmap/ar6	
Figure 7.7		Code	notebooks/220_chapter7_fig7.7.ipynb	MIT	(Smith et al., 2021)	https://github.com/chrisroadmap/ar6	
Figure 7.8		Code	notebooks/230_chapter7_fig7.8.ipynb	MIT	(Smith et al., 2021)	https://github.com/chrisroadmap/ar6	

Cross Chapter Box 7.1 Figure 7.1		Code	notebooks/box-7-1-figure-1/110_plot_box_7-1_emulator_overview_figure_projections_panels.ipynb		(Nicholls et al., 2021)	https://gitlab.com/magicc/ar6-wg1	
Cross Chapter Box 7.1 Figure 7.1	Model datasets	Data	All below models use historical and ssp126 ACCESS-CM2 r1i1p1f1 ACCESS-ESM1-5 r1i1p1f1 BCC-CSM2-MR r1i1p1f1 CESM2 r4i1p1f1 CESM2-WACCM r1i1p1f1 CMCC-CM2-SR5			https://esgf-node.llnl.gov/search/cmip6/	

			r1i1p1f1 CNRM-CM6-1 r1i1p1f2 CNRM-CM6-1-HR r1i1p1f2 CNRM-ESM2-1 r1i1p1f2 CanESM5 r1i1p1f1 CanESM5-CanOE r1i1p2f1 FGOALS-g3 r1i1p1f1 GISS-E2-1-G r1i1p1f2 IPSL-CM6A-LR				

			r1i1p1f2 MIROC-ES2L r1i1p1f2 MIROC6 r1i1p1f1 MPI-ESM1-2-LR r1i1p1f1 MRI-ESM2-0 r1i1p1f1 UKESM1-0-LL r4i1p1f2				
Cross Chapter Box 7.1 Figure 7.1		Data	data/raw/fair/v20210211/scmdatabase/FaIRv1.6.2 data/raw/cicero/2.0.1/scmdatabase/Cicero-SCM data/raw/magicc/v			https://gitlab.com/magicc/ar6-wg1	(Meinshausen et al., 2011a; Gasser et al., 2017a; Smith et al., 2018a; Nicholls et al., 2020)

			20210217/output_210_idealised_experiments_2021_02_17_230201/MAGICCv7.5.1 data/raw/oscar/v20210217/scmdatabase/OSCARv3.1.1				
Figure 7.10		Code	AR6_fbk_violin_plot.py	MIT	(Zelinka, 2021)	https://github.com/mzelinka/AR6_figure	
Figure 7.10		Data	cmip56_feedbacks_AR6.json			https://github.com/mzelinka/AR6_figure	(Zelinka et al., 2020)
Figure 7.11	non-linearity in alpha	Code	nonlin/nonlin_fgd.pro		(Lunt, 2021)	https://github.com/danlunt1976/	
Figure 7.11		Data					Models: (Caballero and Huber, 2013; Jonko et al., 2013; Meraner et al., 2013; Good et al., 2015; Duan et al., 2019; Mauritsen et al., 2019; Stolpe et al., 2019; Zhu et

							al., 2019) Proxies: (von der Heydt et al., 2014; Anagnostou et al., 2016, 2020; Friedrich et al., 2016; Royer, 2016; Shaffer et al., 2016; Köhler et al., 2017; Snyder, 2019; Stap et al., 2019)
Figure 7.13	paleo polar amplification	Code	patterns/fgd/plot_all_fgd.pro		(Lunt, 2021)	https://github.com/danlunt1976/ipcc_ar6	
Figure 7.13		Data					Paleo models: (Haywood et al., 2020; Zhu et al., 2020, 2021; Kageyama et al., 2021; Lunt et al., 2021; Zhang et al., 2021) Proxies: (Bartlein et al., 2011; Salzmann et

							al., 2013; Vieira et al., 2018; Hollis et al., 2019; Cleator et al., 2020; McClymont et al., 2020; Tierney et al., 2020)
Figure 7.16		Code	notebooks/020_chapter7_fig7.16.ipynb	MIT	(Smith et al., 2021)	https://github.com/chrisroadmap/ar6	
Figure 7.17		Code	contributed/fig7.17/tcr_fgd.f	MIT	(Smith et al., 2021) [original author Masahiro Watanabe]	https://github.com/chrisroadmap/ar6	
Figure 7.17		Data					(Geoffroy et al., 2013a; Smith et al., 2020)
Figure 7.18		Code	notebooks/330_chapter7_fig7.18.ipynb	MIT	(Smith et al., 2021) [original author Piers Forster]	https://github.com/chrisroadmap/ar6	
Figure 7.18		Data	data_input/Schlund_et_al_2020				(Schlund et al., 2020)
Figure 7.19		Code	patterns/fgd/plot_all_fgd.pro		(Lunt, 2021)	https://github.com/danlunt1976/ipcc	

						_ar6	
Figure 7.19		Data					(Haywood et al., 2020; Zhu et al., 2020, 2021; Kageyama et al., 2021; Lunt et al., 2021; Zhang et al., 2021)
Figure 7.21		Code	notebooks/320_chapter7_fig7.21.ipynb	MIT	(Smith et al., 2021) [original author William Collins]	https://github.com/chrisroadmap/ar6	
Figure 7.21		Data	data_input/fig7.20				
Figure 7.22		Code	notebooks/310_chapter7_fig7.22.ipynb	MIT	(Smith et al., 2021) [original authors Piers Forster and Michelle Cain]	https://github.com/chrisroadmap/ar6	
Figure 7.22		Data			(Nicholls and Lewis, 2021)	https://doi.org/10.5281/zenodo.4589756	
FAQ 7.3 Figure 1	CDO commands and Python to plot the data points	Code	contributed/faq7.3_fig1	MIT	(Smith et al., 2021) [original author Sophie Berger]	https://github.com/chrisroadmap/ar6	

FAQ 7.3 Figure 1	Input is ECS for each model and projected 2081-2100 global warming in RCP8.5 and SSP5-8.5 respectively: 69 CMIP5 and CMIP6 model outputs	Data	contributed/faq7.3_fig1			https://esgf-data.dkrz.de/ [original data from] https://github.com/chrisroadmap/ar6 [processed data stored at]	(Schlund et al., 2020)

[END TABLE 7.SM.14 HERE]

References

Allen, R. J., Horowitz, L. W., Naik, V., Oshima, N., O'Connor, F. M., Turnock, S., et al. (2021). Significant climate benefits from near-term climate forcer mitigation in spite of aerosol reductions. *Environ. Res. Lett.* doi:10.1088/1748-9326/abe06b.

Anagnostou, E., John, E. H., Babila, T. L., Sexton, P. F., Ridgwell, A., Lunt, D. J., et al. (2020). Proxy evidence for state-dependence of climate sensitivity in the Eocene greenhouse. *Nat. Commun.* 11, 4436. doi:10.1038/s41467-020-17887-x.

Anagnostou, E., John, E. H., Edgar, K. M., Foster, G. L., Ridgwell, A., Inglis, G. N., et al. (2016). Changing atmospheric CO2 concentration was the primary driver of early Cenozoic climate. *Nature* 533, 380–384. doi:10.1038/nature17423.

Arora, V. K., Katavouta, A., Williams, R. G., Jones, C. D., Brovkin, V., Friedlingstein, P., et al. (2020). Carbon-concentration and carbon-climate feedbacks in CMIP6 models and their comparison to CMIP5 models. *Biogeosciences* 17, 4173–4222. doi:10.5194/bg-17-4173-2020.

Bartlein, P. J., Harrison, S. P., Brewer, S., Connor, S., Davis, B. A. S., Gajewski, K., et al. (2011). Pollen-based continental climate reconstructions at 6 and 21 ka: a global synthesis. *Clim. Dyn.* 37, 775–802. doi:10.1007/s00382-010-0904-1.

Caballero, R., and Huber, M. (2013). State-dependent climate sensitivity in past warm climates and its implications for future climate projections. *Proc. Natl. Acad. Sci.* 110, 14162–14167. doi:10.1073/pnas.1303365110.

Checa-Garcia, R., Hegglin, M. I., Kinnison, D., Plummer, D. A., and Shine, K. P. (2018). Historical Tropospheric and Stratospheric Ozone Radiative Forcing Using the CMIP6 Database. *Geophys. Res. Lett.* 45, 3264–3273. doi:10.1002/2017GL076770.

Cleator, S. F., Harrison, S. P., Nichols, N. K., Prentice, I. C., and Roulstone, I. (2020). A new multivariable benchmark for Last Glacial Maximum climate simulations. *Clim. Past* 16, 699–712. doi:10.5194/cp-16-699-2020.

Collins, W. J., Lamarque, J. F., Schulz, M., Boucher, O., Eyring, V., Hegglin, I. M., et al. (2017). AerChemMIP: Quantifying the effects of chemistry and aerosols in CMIP6. *Geosci. Model Dev.* 10, 585–607. doi:10.5194/gmd-10-585-2017.

Duan, L., Cao, L., and Caldeira, K. (2019). Estimating Contributions of Sea Ice and Land Snow to Climate Feedback. *J. Geophys. Res. Atmos.* 124, 199–208. doi:10.1029/2018JD029093.

Etminan, M., Myhre, G., Highwood, E. J., and Shine, K. P. (2016). Radiative forcing of carbon dioxide, methane, and nitrous oxide: A significant revision of the methane radiative forcing. *Geophys. Res. Lett.* 43, 12,614-12,623. doi:10.1002/2016GL071930.

Eyring, V., Bock, L., Lauer, A., Righi, M., Schlund, M., Andela, B., et al. (2020). Earth System Model Evaluation Tool (ESMValTool) v2.0 - An extended set of large-scale diagnostics for quasi-operational and comprehensive evaluation of Earth system models in CMIP. *Geosci. Model Dev.* 13, 3383–3438. doi:10.5194/gmd-13-3383-2020.

Eyring, V., Bony, S., Meehl, G. A., Senior, C. A., Stevens, B., Stouffer, R. J., et al. (2016). Overview of the Coupled Model Intercomparison Project Phase 6 (CMIP6) experimental design and organization. *Geosci. Model Dev.* 9, 1937–1958. doi:10.5194/gmd-9-1937-2016.

Friedrich, T., Timmermann, A., Tigchelaar, M., Timm, O. E., and Ganopolski, A. (2016). Nonlinear climate sensitivity and its implications for future greenhouse warming. *Sci. Adv.* 2. doi:10.1126/sciadv.1501923.

Gasser, T., Ciais, P., Boucher, O., Quilcaille, Y., Tortora, M., Bopp, L., et al. (2017a). The compact Earth system model OSCAR v2.2: Description and first results. *Geosci. Model Dev.* 10, 271–319. doi:10.5194/gmd-10-271-2017.

Gasser, T., Peters, G. P., Fuglestvedt, J. S., Collins, W. J., Shindell, D. T., and Ciais, P. (2017b). Accounting for the climate–carbon feedback in emission metric. *Earth Syst. Dyn.* 8, 235–253. doi:10.5194/esd-8-235-2017.

Geoffroy, O., Saint-Martin, D., Bellon, G., Voldoire, A., Olivié, D. J. L. L., and Tytéca, S. (2013a). Transient Climate Response in a Two-Layer Energy-Balance Model. Part II: Representation of the Efficacy of Deep-Ocean Heat Uptake and Validation for CMIP5 AOGCMs. *J. Clim.* 26, 1859–1876. doi:10.1175/JCLI-D-12-00196.1.

Geoffroy, O., Saint-martin, D., Olivié, D. J. L., Voldoire, A., Bellon, G., and Tytéca, S. (2013b). Transient climate response in a two-layer energy-balance model. Part I: Analytical solution and parameter calibration using CMIP5 AOGCM experiments. *J. Clim.* 26, 1841–1857. doi:10.1175/JCLI-D-12-00195.1.

Ghan, S. J., Smith, S. J., Wang, M., Zhang, K., Pringle, K., Carslaw, K., et al. (2013). A simple model of global aerosol indirect effects. *J. Geophys. Res. Atmos.* 118, 6688–6707. doi:10.1002/jgrd.50567.

Ghimire, B., Williams, C. A., Masek, J., Gao, F., Wang, Z., Schaaf, C., et al. (2014). Global albedo change and radiative cooling from anthropogenic land cover change, 1700 to 2005 based on MODIS, land use harmonization, radiative kernels, and reanalysis. *Geophys. Res. Lett.* doi:10.1002/2014GL061671.

Gidden, M. J., Riahi, K., Smith, S. J., Fujimori, S., Luderer, G., Kriegler, E., et al. (2019). Global emissions pathways under different socioeconomic scenarios for use in CMIP6: a dataset of harmonized emissions trajectories through the end of the century. *Geosci. Model Dev.* 12, 1443–1475. doi:10.5194/gmd-12-1443-2019.

Good, P., Lowe, J. A., Andrews, T., Wiltshire, A., Chadwick, R., Ridley, J. K., et al. (2015). Nonlinear regional

warming with increasing CO2 concentrations. *Nat. Clim. Chang.* 5, 138–142. doi:10.1038/nclimate2498.
Gregory, J. M., Andrews, T., and Good, P. (2015). The inconstancy of the transient climate response parameter under increasing CO2. *Philos. Trans. R. Soc. A Math. Phys. Eng. Sci.* 373. doi:10.1098/rsta.2014.0417.
Gregory, J. M., Ingram, W. J., Palmer, M. A., Jones, G. S., Stott, P. A., Thorpe, R. B., et al. (2004). A new method for diagnosing radiative forcing and climate sensitivity. *Geophys. Res. Lett.* 31, L03205. doi:10.1029/2003GL018747.
Haywood, A. M., Tindall, J. C., Dowsett, H. J., Dolan, A. M., Foley, K. M., Hunter, S. J., et al. (2020). The Pliocene Model Intercomparison Project Phase 2: large-scale climate features and climate sensitivity. *Clim. Past* 16, 2095–2123. doi:10.5194/cp-16-2095-2020.
Hodnebrog, Ø., Myhre, G., Kramer, R. J., Shine, K. P., Andrews, T., Faluvegi, G., et al. (2020). The effect of rapid adjustments to halocarbons and N2O on radiative forcing. *npj Clim. Atmos. Sci.* 3. doi:https://doi.org/10.1038/s41612-020-00150-x.
Hoesly, R. M., Smith, S. J., Feng, L., Klimont, Z., Janssens-Maenhout, G., Pitkanen, T., et al. (2018). Historical (1750–2014) anthropogenic emissions of reactive gases and aerosols from the Community Emissions Data System (CEDS). *Geosci. Model Dev.* 11, 369–408. doi:10.5194/gmd-11-369-2018.
Hollis, C. J., Dunkley Jones, T., Anagnostou, E., Bijl, P. K., Cramwinckel, M. J., Cui, Y., et al. (2019). The DeepMIP contribution to PMIP4: methodologies for selection, compilation and analysis of latest Paleocene and early Eocene climate proxy data, incorporating version 0.1 of the DeepMIP database. *Geosci. Model Dev.* 12, 3149–3206. doi:10.5194/gmd-12-3149-2019.
Jiménez-de-la-Cuesta, D., and Mauritsen, T. (2019). Emergent constraints on Earth's transient and equilibrium response to doubled CO2 from post-1970s global warming. *Nat. Geosci.* 2015. doi:10.1038/s41561-019-0463-y.
Jonko, A. K., Shell, K. M., Sanderson, B. M., and Danabasoglu, G. (2013). Climate Feedbacks in CCSM3 under Changing CO2 Forcing. Part II: Variation of Climate Feedbacks and Sensitivity with Forcing. *J. Clim.* 26, 2784–2795. doi:10.1175/JCLI-D-12-00479.1.
Joos, F., Roth, R., Fuglestvedt, J. S., Peters, G. P., Enting, I. G., Von Bloh, W., et al. (2013). Carbon dioxide and climate impulse response functions for the computation of greenhouse gas metrics: A multi-model analysis. *Atmos. Chem. Phys.* 13, 2793–2825. doi:10.5194/acp-13-2793-2013.
Jungclaus, J. H., Bard, E., Baroni, M., Braconnot, P., Cao, J., Chini, L. P., et al. (2017). The PMIP4 contribution to CMIP6 Part 3: The last millennium, scientific objective, and experimental design for PMIP4 simulations. *Geosci. Model Dev.* 10, 4005–4033. doi:10.5194/gmd-10-4005-2017.
Kageyama, M., Harrison, S. P., Kapsch, M. M.-L., Löfverström, M., Lora, J. M., Mikolajewicz, U., et al. (2021). The PMIP4-CMIP6 Last Glacial Maximum experiments: preliminary results and comparison with the PMIP3-CMIP5 simulations. *Clim. Past*, 1–37. doi:10.5194/cp-2019-169.
Kanaya, Y., Yamaji, K., Miyakawa, T., Taketani, F., Zhu, C., Choi, Y., et al. (2020). Rapid reduction in black carbon emissions from China: Evidence from 2009-2019 observations on Fukue Island, Japan. *Atmos. Chem. Phys.* 20, 6339–6356. doi:10.5194/acp-20-6339-2020.
Köhler, P., Stap, L. B., von der Heydt, A. S., de Boer, B., Van De Wal, R. S. W., and Bloch-Johnson, J. (2017). A state-dependent quantification of climate sensitivity based on paleo data of the last 2.1 million years. *Paleoceanography*, 1–13. doi:10.1002/2017PA003190.
Kovilakam, M., Thomason, L. W., Ernest, N., Rieger, L., Bourassa, A., and Millán, L. (2020). The Global Space-based Stratospheric Aerosol Climatology (version 2.0): 1979–2018. *Earth Syst. Sci. Data* 12, 2607–2634. doi:10.5194/essd-12-2607-2020.
Lauer, A., Eyring, V., Bellprat, O., Bock, L., Gier, B. K., Hunter, A., et al. (2020). Earth System Model Evaluation Tool (ESMValTool) v2.0 - Diagnostics for emergent constraints and future projections from Earth system models in CMIP. *Geosci. Model Dev.* 13, 4205–4228. doi:10.5194/gmd-13-4205-2020.
Lee, D. S. S., Fahey, D. W. W., Skowron, A., Allen, M. R. R., Burkhardt, U., Chen, Q., et al. (2020). The contribution of global aviation to anthropogenic climate forcing for 2000 to 2018. *Atmos. Environ.* 244. doi:10.1016/j.atmosenv.2020.117834.
Loeb, N. G., Wang, H., Allan, R., Andrews, T., Armour, K., Cole, J. N. S., et al. (2020). New Generation of Climate Models Track Recent Unprecedented Changes in Earth's Radiation Budget Observed by CERES. *Geophys. Res. Lett.* 47. doi:10.1029/2019GL086705.
Lunt, D. J. (2021). Code and data for Chapter 7.
Lunt, D. J., Bragg, F., Chan, W. L. W.-L., Hutchinson, D. K., Ladant, J. J.-B. B. J.-B., Niezgodzki, I., et al. (2021). DeepMIP: Model intercomparison of early Eocene climatic optimum (EECO) large-scale climate features and comparison with proxy data. *Clim. Past* 17, 203–227. doi:10.5194/cp-17-203-2021.
Marshall, L. R., Smith, C. J., Forster, P. M., Schmidt, A., Aubry, T. J., Andrews, T., et al. (2020). Large Variations in Volcanic Aerosol Forcing Efficiency Due to Eruption Source Parameters and Rapid Adjustments. *Geophys. Res. Lett.* 47. doi:10.1029/2020GL090241.
Matthes, K., Funke, B., Andersson, M. E., Barnard, L., Beer, J., Charbonneau, P., et al. (2017). Solar forcing for CMIP6 (v3.2). *Geosci. Model Dev.* 10, 2247–2302. doi:10.5194/gmd-10-2247-2017.
Mauritsen, T., Bader, J., Becker, T., Behrens, J., Bittner, M., Brokopf, R., et al. (2019). Developments in the MPI-M

Earth System Model version 1.2 (MPI-ESM 1.2) and its response to increasing CO2. *J. Adv. Model. Earth Syst.* 0. doi:10.1029/2018MS001400.

McClymont, E. L., Ford, H. L., Ho, S. L., Tindall, J. C., Haywood, A. M., Alonso-Garcia, M., et al. (2020). Lessons from a high-CO2 world: an ocean view from ~3 million years ago. *Clim. Past* 16, 1599–1615. doi:10.5194/cp-16-1599-2020.

Meehl, G. A., Senior, C. A., Eyring, V., Flato, G., Lamarque, J.-F., Stouffer, R. J., et al. (2020). Context for interpreting equilibrium climate sensitivity and transient climate response from the CMIP6 Earth system models. *Sci. Adv.* 6. doi:10.1126/sciadv.aba1981.

Meinshausen, M., Nicholls, Z. R. J., Lewis, J., Gidden, M. J., Vogel, E., Freund, M., et al. (2020). The shared socio-economic pathway (SSP) greenhouse gas concentrations and their extensions to 2500. *Geosci. Model Dev.* 13, 3571–3605. doi:10.5194/gmd-13-3571-2020.

Meinshausen, M., Raper, S. C. B. B., and Wigley, T. M. L. L. (2011a). Emulating coupled atmosphere-ocean and carbon cycle models with a simpler model, MAGICC6 – Part 1: Model description and calibration. *Atmos. Chem. Phys.* 11, 1417–1456. doi:10.5194/acp-11-1417-2011.

Meinshausen, M., Smith, S. J., Calvin, K., Daniel, J. S., Kainuma, M. L. T., Lamarque, J., et al. (2011b). The RCP greenhouse gas concentrations and their extensions from 1765 to 2300. *Clim. Change* 109, 213–241. doi:10.1007/s10584-011-0156-z.

Meinshausen, M., Vogel, E., Nauels, A., Lorbacher, K., Meinshausen, N., Etheridge, D. M., et al. (2017). Historical greenhouse gas concentrations for climate modelling (CMIP6). *Geosci. Model Dev.* 10, 2057–2116. doi:10.5194/gmd-10-2057-2017.

Meraner, K., Mauritsen, T., and Voigt, A. (2013). Robust increase in equilibrium climate sensitivity under global warming. *Geophys. Res. Lett.* 40, 5944–5948. doi:10.1002/2013GL058118.

Millar, J. R., Nicholls, Z. R., Friedlingstein, P., and Allen, M. R. (2017). A modified impulse-response representation of the global near-surface air temperature and atmospheric concentration response to carbon dioxide emissions. *Atmos. Chem. Phys.* 17, 7213–7228. doi:10.5194/acp-17-7213-2017.

Myhre, G., Highwood, E. J., Shine, K. P., and Stordal, F. (1998). New estimates of radiative forcing due to well mixed greenhouse gases. *Geophys. Res. Lett.* 25, 2715–2718. doi:10.1029/98GL01908.

Myhre, G., Samset, B. H., Schulz, M., Balkanski, Y., Bauer, S., Berntsen, T. K., et al. (2013a). Radiative forcing of the direct aerosol effect from AeroCom Phase II simulations. *Atmos. Chem. Phys.* 13, 1853–1877. doi:10.5194/acp-13-1853-2013.

Myhre, G., Shindell, D., Bréon, F.-M., Collins, W., Fuglestvedt, J., Huang, J., et al. (2013b). "Anthropogenic and Natural Radiative Forcing," in *Climate Change 2013: The Physical Science Basis. Contribution of Working Group I to the Fifth Assessment Report of the Intergovernmental Panel on Climate Change*, eds. T. F. Stocker, D. Qin, G.-K. Plattner, M. Tignor, S. K. Allen, J. Boschung, et al. (Cambridge, United Kingdom and New York, NY, USA: Cambridge University Press), 659–740. doi:10.1017/ CBO9781107415324.018.

Newman, P. A., Daniel, J. S., Waugh, D. W., and Nash, E. R. (2007). A new formulation of equivalent effective stratospheric chlorine (EESC). *Atmos. Chem. Phys.* 7, 4537–4552. doi:10.5194/acp-7-4537-2007.

Nicholls, Z., and Lewis, J. (2021). Reduced Complexity Model Intercomparison Project (RCMIP) protocol. doi:10.5281/ZENODO.4589756.

Nicholls, Z., Lewis, J., and Meinshausen, M. (2021). Code and data for Cross Chapter Box 7.1.

Nicholls, Z. R. J., Meinshausen, M., Lewis, J. J., Gieseke, R., Dommenget, D., Dorheim, K., et al. (2020). Reduced Complexity Model Intercomparison Project Phase 1: introduction and evaluation of global-mean temperature response. *Geosci. Model Dev.* 13, 5175–5190. doi:10.5194/gmd-13-5175-2020.

Paulot, F., Paynter, D., Ginoux, P., Naik, V., and Horowitz, L. W. (2018). Changes in the aerosol direct radiative forcing from 2001 to 2015: Observational constraints and regional mechanisms. *Atmos. Chem. Phys.* 18, 13265–13281. doi:10.5194/acp-18-13265-2018.

Riahi, K., Rao, S., Krey, V., Cho, C., Chirkov, V., Fischer, G., et al. (2011). RCP 8.5-A scenario of comparatively high greenhouse gas emissions. *Clim. Change* 109, 33–57. doi:10.1007/s10584-011-0149-y.

Righi, M., Andela, B., Eyring, V., Lauer, A., Predoi, V., Schlund, M., et al. (2020). Earth System Model Evaluation Tool (ESMValTool) v2.0-technical overview. *Geosci. Model Dev.* 13, 1179–1199. doi:10.5194/gmd-13-1179-2020.

Royer, D. L. (2016). Climate Sensitivity in the Geologic Past. *Annu. Rev. Earth Planet. Sci.* 44, 277–293. doi:10.1146/annurev-earth-100815-024150.

Salzmann, U., Dolan, A. M., Haywood, A. M., Chan, W. Le, Voss, J., Hill, D. J., et al. (2013). Challenges in quantifying Pliocene terrestrial warming revealed by data-model discord. *Nat. Clim. Chang.* 3, 969–974. doi:10.1038/nclimate2008.

Schlund, M., Lauer, A., Gentine, P., Sherwood, S., and Eyring, V. (2020). Emergent constraints on Equilibrium Climate Sensitivity in CMIP5: do they hold for CMIP6? *Earth Syst. Dyn.* 11, 1233–1258. doi:https://doi.org/10.5194/esd-11-1233-2020.

Shaffer, G., Huber, M., Rondanelli, R., and Pepke Pedersen, J. O. (2016). Deep time evidence for climate sensitivity increase with warming. *Geophys. Res. Lett.* 43, 6538–6545. doi:10.1002/2016GL069243.

Sherwood, S. C., Dixit, V., and Salomez, C. (2018). The global warming potential of near-surface emitted water vapour. *Environ. Res. Lett.* doi:10.1088/1748-9326/aae018.
Skeie, R. B., Myhre, G., Hodnebrog, Ø., Cameron-Smith, P. J., Deushi, M., Hegglin, M. I., et al. (2020). Historical total ozone radiative forcing derived from CMIP6 simulations. *npj Clim. Atmos. Sci.* doi:10.1038/s41612-020-00131-0.
Smith, C. J., Berger, S., Cain, M., Collins, W. J., Forster, P. M., Harris, G. R., et al. (2021). Code and data for Chapter 7.
Smith, C. J., Forster, P. M., Allen, M., Leach, N., Millar, R. J., Passerello, G. A., et al. (2018a). FAIR v1.3: A simple emissions-based impulse response and carbon cycle model. *Geosci. Model Dev.* doi:10.5194/gmd-11-2273-2018.
Smith, C. J., Kramer, R. J., Myhre, G., Alterskjær, K., Collins, W., Sima, A., et al. (2020). Effective radiative forcing and adjustments in CMIP6 models. *Atmos. Chem. Phys.* 20, 9591–9618. doi:10.5194/acp-20-9591-2020.
Smith, C. J., Kramer, R. J., Myhre, G., Forster, P. M., Soden, B. J., Andrews, T., et al. (2018b). Understanding Rapid Adjustments to Diverse Forcing Agents. *Geophys. Res. Lett.* 45. doi:10.1029/2018GL079826.
Snyder, C. W. (2019). Revised estimates of paleoclimate sensitivity over the past 800,000 years. *Clim. Change* 156, 121–138. doi:10.1007/s10584-019-02536-0.
Stap, L. B., Köhler, P., and Lohmann, G. (2019). Including the efficacy of land ice changes in deriving climate sensitivity from paleodata. *Earth Syst. Dyn.* 10, 333–345. doi:10.5194/esd-10-333-2019.
Sterner, E., Johansson, D. J. A., and Azar, C. (2014). Emission metrics and sea level rise. *Clim. Change* 127, 335–351. doi:10.1007/s10584-014-1258-1.
Stevens, B. (2015). Rethinking the lower bound on aerosol radiative forcing. *J. Clim.* 28, 4794–4819. doi:10.1175/JCLI-D-14-00656.1.
Stevenson, D. S., Young, P. J., Naik, V., Lamarque, J.-F., Shindell, D. T., Voulgarakis, A., et al. (2013). Tropospheric ozone changes, radiative forcing and attribution to emissions in the Atmospheric Chemistry and Climate Model Intercomparison Project (ACCMIP). *Atmos. Chem. Phys.* 13, 3063–3085. doi:10.5194/acp-13-3063-2013.
Stolpe, M. B., Medhaug, I., Beyerle, U., and Knutti, R. (2019). Weak dependence of future global mean warming on the background climate state. *Clim. Dyn.* 53, 5079–5099. doi:10.1007/s00382-019-04849-3.
Thornhill, G., Collins, W., Olivié, D., Skeie, R. B., Archibald, A., Bauer, S., et al. (2021a). Climate-driven chemistry and aerosol feedbacks in CMIP6 Earth system models. *Atmos. Chem. Phys.* 21, 1105–1126. doi:10.5194/acp-21-1105-2021.
Thornhill, G. D., Collins, W. J., Kramer, R. J., Olivie, D., Skeie, R. B., O'Connor, F. M., et al. (2021b). Effective radiative forcing from emissions of reactive gases and aerosols-A multi-model comparison. *Atmos. Chem. Phys.* 21, 853–874. doi:10.5194/acp-21-853-2021.
Tierney, J. E., Poulsen, C. J., Montañez, I. P., Bhattacharya, T., Feng, R., Ford, H. L., et al. (2020). Past climates inform our future. *Science (80-.).* 370. doi:10.1126/science.aay3701.
Toohey, M., and Sigl, M. (2017). Volcanic stratospheric sulfur injections and aerosol optical depth from 500 BCE to 1900 CE. *Earth Syst. Sci. Data* 9, 809–831. doi:10.5194/essd-9-809-2017.
Van Marle, M. J. E., Kloster, S., Magi, B. I., Marlon, J. R., Daniau, A. L., Field, R. D., et al. (2017). Historic global biomass burning emissions for CMIP6 (BB4CMIP) based on merging satellite observations with proxies and fire models (1750-2015). *Geosci. Model Dev.* 10, 3329–3357. doi:10.5194/gmd-10-3329-2017.
Velders, G. J. M., Fahey, D. W., Daniel, J. S., Andersen, S. O., and McFarland, M. (2015). Future atmospheric abundances and climate forcings from scenarios of global and regional hydrofluorocarbon (HFC) emissions. *Atmos. Environ.* 123, 200–209. doi:https://doi.org/10.1016/j.atmosenv.2015.10.071.
Vieira, M., Pound, M. J., and Pereira, D. I. (2018). The late Pliocene palaeoenvironments and palaeoclimates of the western Iberian Atlantic margin from the Rio Maior flora. *Palaeogeogr. Palaeoclimatol. Palaeoecol.* 495, 245–258. doi:10.1016/j.palaeo.2018.01.018.
von der Heydt, A. S., Dijkstra, H. A., Köhler, P., and Wal, R. Van De (2014). On the background state dependency of (palaeo) climate sensitivity. *Geophys. Res. Lett.* 41, 6484–6492. doi:10.1002/2014GL061121.
Zelinka, M. D. (2021). IPCC AR6 Figure 7.10.
Zelinka, M. D., Andrews, T., Forster, P. M., and Taylor, K. E. (2014). Quantifying components of aerosol-cloud-radiation interactions in climate models. *J. Geophys. Res. Atmos.* 119, 7599–7615. doi:10.1002/2014JD021710.
Zelinka, M. D., Myers, T. A., McCoy, D. T., Po-Chedley, S., Caldwell, P. M., Ceppi, P., et al. (2020). Causes of higher climate sensitivity in CMIP6 models. *Geophys. Res. Lett.* 46, 2019GL085782. doi:10.1029/2019GL085782.
Zhang, Z., Li, X., Guo, C., Otterå, O. H., Nisancioglu, K. H., Tan, N., et al. (2021). Mid-Pliocene Atlantic Meridional Overturning Circulation simulated in PlioMIP2. *Clim. Past* 17, 529–543. doi:10.5194/cp-17-529-2021.
Zhu, J., Otto-Bliesner, B. L., Brady, E. C., Poulsen, C. J., Tierney, J. E., Lofverstrom, M., et al. (2021). Assessment of Equilibrium Climate Sensitivity of the Community Earth System Model Version 2 Through Simulation of the Last Glacial Maximum. *Geophys. Res. Lett.* 48, e2020GL091220. doi:10.1029/2020GL091220.
Zhu, J., Poulsen, C. J., and Otto-Bliesner, B. L. (2020). High climate sensitivity in CMIP6 model not supported by paleoclimate. *Nat. Clim. Chang.* 10, 378–379. doi:10.1038/s41558-020-0764-6.
Zhu, J., Poulsen, C. J., and Tierney, J. E. (2019). Simulation of Eocene extreme warmth and high climate sensitivity through cloud feedbacks. *Sci. Adv.* 5. doi:10.1126/sciadv.aax1874.